

Quantitative phosphoproteomic analysis reveals common regulatory mechanisms between effector- and PAMP-triggered immunity in plants

Yasuhiro Kadota^{1*} , Thomas W. H. Liebrand^{2*} , Yukihisa Goto¹ , Jan Sklenar³ , Paul Derbyshire³ , Frank L. H. Menke³ , Miguel-Angel Torres^{4,5} , Antonio Molina^{4,5} , Cyril Zipfel^{3,6} , Gitta Coaker²  and Ken Shirasu¹ 

¹RIKEN Center for Sustainable Resource Science, Plant Immunity Research Group, Suehiro-cho 1-7-22 Tsurumi-ku, Yokohama 230-0045, Japan; ²Department of Plant Pathology, University of California Davis, One Shields Avenue, Davis, CA 95616, USA; ³The Sainsbury Laboratory, Norwich Research Park, Norwich, NR4 7UH, UK; ⁴Centro de Biotecnología y Genómica de Plantas, Universidad Politécnica de Madrid (UPM)-Instituto Nacional de Investigación y Tecnología Agraria y Alimentaria (INIA), Campus Montegancedo UPM, 28223 Pozuelo de Alarcón (Madrid), Spain; ⁵Departamento de Biotecnología-Biología Vegetal, Escuela Técnica Superior de Ingeniería Agronómica, Alimentaria y de Biosistemas, Universidad Politécnica de Madrid, 28040 Madrid, Spain; ⁶Department of Molecular and Cellular Plant Physiology, University of Zurich, Zollikerstrasse 107, CH-8008 Zurich, Switzerland

Summary

Authors for correspondence:

Ken Shirasu

Tel: +81 45 503 9574

Email: ken.shirasu@riken.jp

Gitta Coaker

Tel: +1 530 752 6541

Email: gcoaker@ucdavis.edu

Received: 30 July 2018

Accepted: 1 October 2018

New Phytologist (2018)

doi: 10.1111/nph.15523

Key words: *Arabidopsis*, bacteria, effectors, fungi, pathogen-associated molecular patterns (PAMPs), plant immunity, protein phosphorylation, reactive oxygen species (ROS).

- Plant immunity consists of two arms: pathogen-associated molecular pattern (PAMP)-triggered immunity (PTI), induced by surface-localized receptors, and effector-triggered immunity (ETI), induced by intracellular receptors. Despite the little structural similarity, both receptor types activate similar responses with different dynamics.
- To better understand phosphorylation events during ETI, we employed a phosphoproteomic screen using an inducible expression system of the bacterial effector *avrRpt2* in *Arabidopsis thaliana*, and identified 109 differentially phosphorylated residues of membrane-associated proteins on activation of the intracellular RPS2 receptor.
- Interestingly, several RPS2-regulated phosphosites overlap with sites that are regulated during PTI, suggesting that these phosphosites may be convergent points of both signaling arms. Moreover, some of these sites are residues of important defense components, including the NADPH oxidase RBOHD, ABC-transporter PEN3, calcium-ATPase ACA8, noncanonical G α protein XLG2 and H⁺-ATPases. In particular, we found that S343 and S347 of RBOHD are common phosphorylation targets during PTI and ETI. Our mutational analyses showed that these sites are required for the production of reactive oxygen species during both PTI and ETI, and immunity against avirulent bacteria and a virulent necrotrophic fungus.
- We provide, for the first time, large-scale phosphoproteomic data of ETI, thereby suggesting crucial roles of common phosphosites in plant immunity.

Introduction

The recognition of pathogenic microorganisms is the first crucial step in the immune response of plants aimed at the inhibition of pathogen ingress. Typically, the plant immune system is represented by two distinct arms (Jones & Dangl, 2006; Dodds & Rathjen, 2010). The first arm is initiated on perception of pathogen-associated molecular patterns (PAMPs) by cell surface-localized pattern recognition receptors (PRRs), leading to PAMP-triggered immunity (PTI). Plant PRRs are either receptor-like kinases (RLKs) or receptor-like proteins (Boutrot & Zipfel, 2017). Successful pathogens cause disease using effector molecules that interfere with PTI. Bacterial effectors are often

proteins secreted into plant cells via the type III secretion system. For example, the pathogen effector AvrRpm1 from *Pseudomonas syringae* pv *maculicola*, as well as AvrB and AvrRpt2 from *Pseudomonas syringae* pv *tomato* (*Pto*), target the *Arabidopsis* membrane-localized protein RPM1-INTERACTING PROTEIN-4 (RIN4), which is a regulator of PTI (Chung *et al.*, 2014; Lee *et al.*, 2015). Phosphorylation of RIN4 by AvrB through RPM1-INDUCED PROTEIN KINASE (RIPK) and the degradation of RIN4 by AvrRpt2 are recognized by the intracellular nucleotide-binding domain leucine-rich repeat (NLR)-type immune receptors RESISTANCE TO *P. SYRINGAE* PV MACULICOLA-1 (RPM1) and RESISTANT TO *P. SYRINGAE*-2 (RPS2), respectively (Spoel & Dong, 2012; Khan *et al.*, 2016). The activation of NLRs results in effector-triggered immunity (ETI).

*These authors contributed equally to this work.

ETI is considered to be a stronger and faster response than PTI (Jones & Dangl, 2006). PTI and ETI share some signaling components, such as Ca^{2+} and mitogen-activated protein kinase (MAPK) cascades (Tsuda *et al.*, 2013; Yu *et al.*, 2017). In addition, they share immune responses, such as transcriptional reprogramming, the generation of apoplastic reactive oxygen species (ROS), and the production and secretion of antimicrobial compounds. However, the activated immune responses during ETI are generally more prolonged and robust than those during PTI (Dodds & Rathjen, 2010; Tsuda & Katagiri, 2010; Thomma *et al.*, 2011). These observations suggest that the same signaling components or enzymes are similarly regulated during PTI and ETI, whereas the dynamics and strength of the activation are different. However, it is currently unclear how NLRs transduce the signal downstream and how PRRs and NLRs, localized to different cellular compartments, activate similar components to induce related defense outputs.

ROS have various roles in immune signaling and are produced by RESPIRATORY BURST OXIDASE HOMOLOG D (RBOHD) during both PTI and ETI, but with different kinetics: ROS accumulation is only detectable hours after activation of RPM1 and RPS2 by cognate effectors (Torres *et al.*, 2002). Recent research has clarified the molecular mechanisms underlying signaling from PAMP recognition to the ROS burst. On recognition of the flagellin 22 (flg22) peptide, derived from bacterial flagellin, the PRR FLAGELLIN SENSING-2 (FLS2) associates with its coreceptor RLK BRI1-ASSOCIATED RECEPTOR KINASE-1 (BAK1). The FLS2–BAK1 interaction induces the phosphorylation and activation of both proteins, resulting in the phosphorylation of the receptor-like cytoplasmic kinase (RLCK) BOTRYTIS-INDUCED KINASE-1 (BIK1). Subsequently, BIK1 directly phosphorylates RBOHD, responsible for the apoplastic ROS burst observed within minutes after PRR activation (Kadota *et al.*, 2014, 2015; Li *et al.*, 2014). Although phosphorylation-mediated activation of RBOHD has been well studied during PTI, it is currently unknown whether similar RBOHD phosphorylation patterns are induced during ETI.

To gain insights into ETI signaling, we have previously analyzed the changes in abundance of plasma membrane-localized proteins during ETI mediated by RPS2 using transgenic *Arabidopsis* lines expressing the bacterial effector *avrRpt2* under a dexamethasone (Dex)-inducible promoter (McNellis *et al.*, 1998; Elmore *et al.*, 2012). Among the significantly upregulated proteins after activation of RPS2, many proteins belong to the protein kinase superfamily, suggesting that protein phosphorylation plays a crucial role during RPS2-mediated ETI. However, phosphorylation-based regulation of immune regulatory networks during ETI is still largely unknown. Jones *et al.* (2006) examined quantitative changes in the phosphoproteome of *Arabidopsis* infiltrated with *Pto* DC3000 (*avrRpm1*) and found that only one protein (the large subunit of Rubisco) was highly phosphorylated after activation of RPM1, but the exact phosphorylation site was not elucidated. The low success rate of phosphosite identification when avirulent pathogens are used may be a result of the difficulty in synchronously inducing only ETI in sufficient cells without activating PTI.

Here, we employed an unbiased phosphoproteomic screen using an *avrRpt2*-inducible expression system, and successfully identified differentially phosphorylated membrane-associated proteins during the early stages of ETI. Interestingly, several RPS2-regulated phosphorylation sites overlap with sites differentially phosphorylated during PTI as published previously. Our results suggest that these common phosphorylation sites may be convergent points of both immune signaling arms. For example, PAMP-responsive RBOHD phosphorylation sites, S343 and S347, are also highly phosphorylated during ETI. Functional analyses revealed that these RBOHD sites are required for ROS production during both PTI and ETI, as well as for full resistance against avirulent *Pto* strains and a virulent necrotrophic fungus. Our study provides important phosphoproteomic data contributing to our understanding of the ETI signaling network and showing commonalities with and differences from the PTI signaling network.

Materials and Methods

Plant materials and growth conditions

Arabidopsis plants were grown in a controlled growth chamber under 70% relative humidity at 23°C and a light intensity of 85 $\mu\text{mol m}^{-2} \text{s}^{-1}$. A 10-h light and 14-h dark photoperiod was applied. Plant genotypes are described in Supporting Information Methods S1.

Phosphopeptide sample preparation

In each of three biological replicates, flats of *Dex:avrRpt2* and control *rpm1rps2/Dex:avrRpt2 Arabidopsis* plants were grown for 5 wk. Subsequently, plants were sprayed with an aqueous solution containing 30 μM Dex and 0.025% Silwett L-77. In total, 10 g of leaf tissue was harvested per sample at 0, 1 and 3 h after spraying with Dex and flash-frozen in liquid nitrogen. Details of the phosphopeptide enrichment method are described in Methods S1.

LC-MS/MS and data analysis

Phosphopeptide samples were separately analyzed by a QExactive Plus Orbitrap mass spectrometer (Thermo Fisher Scientific, Waltham, MA, USA) LC-MS/MS for a total of 18 runs at the UC Davis Proteomics Core. LC-MS/MS settings and specifics are described in Methods S1. LC-MS/MS raw files were analyzed using the MAXQUANT (v.1.5.1.0) and PERSEUS (v.1.5.0.15) software packages (Tyanova *et al.*, 2016a,b). Raw data files were searched against a FASTA database containing the *Arabidopsis thaliana* proteome. Statistical analysis is described in Methods S1. Raw data and search engine results are available at the PRIDE ProteomeXchange website under accession number PXD010440 (Vizcaino *et al.*, 2013). Details of quantified phosphosites are shown in Tables S1–S4. Search parameters for MAXQUANT can be found in Table S5. Highest intensities and spectra per phosphosite are reported in Table S6.

Selected reaction monitoring (SRM) and data analysis

FLAG-RBOHD proteins extracted from *rbohD/35S:FLAG-RbohD* were immunoprecipitated with anti-FLAG antibody and separated by sodium dodecylsulfate-polyacrylamide gel electrophoresis (SDS-PAGE) (NuPAGE[®]; Invitrogen, Carlsbad, CA, USA). After staining with Coomassie Brilliant Blue G-250 (CBB; SimplyBlue[™] stain; Invitrogen), the proteins were cut out and digested with trypsin, as described previously (Kadota *et al.*, 2014). The intensities of phosphopeptides were normalized by the intensity of control nonphosphorylated RBOHD peptides. Details are provided in Methods S1; the transitions used for SRM are presented in Table S7.

Disease assays

Bacterial disease assays were performed as described previously (Kim *et al.*, 2005). *Plectosphaerella cucumerina* BMM (*PcBMM*) disease assays and fungal biomass determination were performed as described previously (Torres *et al.*, 2013). A detailed description is described in Methods S1. The primers used for quantitative PCR analysis are shown in Table S8.

ROS staining and measurements

The ROS staining protocol was adapted from an earlier described 3,3'-diaminobenzidine (DAB, Sigma) staining protocol (Thordal-Christensen *et al.*, 1997) and is described in detail in Methods S1.

Results

An unbiased phosphoproteomic screen reveals ETI-dependent differential phosphorylation sites

Previous phosphoproteomic studies have identified a large number of differentially phosphorylated proteins during PTI (Benschop *et al.*, 2007; Nühse *et al.*, 2007; Rayapuram *et al.*, 2014; Mattei *et al.*, 2016). To identify differential phosphorylation sites during ETI, we used *Dex:avrRpt2 Arabidopsis* lines to activate RPS2 synchronously and to effectively eliminate the effect of any bacterial PAMPs which would activate PTI. It has been reported that AvrRpt2 can also weakly activate RPM1 (Kim *et al.*, 2009). Therefore, we generated an *rpm1rps2/Dex:avrRpt2* control line which does not induce ETI (Fig. S1a). We confirmed that both lines showed comparable Dex-inducible *avrRpt2* transcript expression and RIN4 protein degradation (Fig. S1b,c). By comparing the two lines, we aimed to identify differentially phosphorylated sites that are dependent on the activation of RPS2.

We decided to analyze membrane fractions because RPS2 associates to the plasma membrane and we expected that early phosphorylation events would occur at the plasma membrane (Qi & Katagiri, 2009). In addition, membrane fractions are less complex in protein composition compared with total protein fractions, thus enabling us to perform label-free quantification using single MS runs. Before or after treatment with Dex for 1 or 3 h,

total membrane fractions of *Dex:avrRpt2* and *rpm1rps2/Dex:avrRpt2* were digested with trypsin, followed by phosphopeptide enrichment using magnetic TiO₂ beads and identification by MS (Fig. 1). Label-free quantitative analysis followed by ANOVA ($P \leq 0.05$) revealed 264 unique phosphorylation sites to be statistically significantly changed in abundance in at least one condition (Table S1). These sites included (1) those regulated by activated RPS2, (2) those regulated by AvrRpt2 independent of RPS2 activation, (3) those regulated by Dex treatment independently of AvrRpt2 and/or RPS2, and (4) those differentially phosphorylated solely depending on the plant genotype. To extract differentially phosphorylated sites after *avrRpt2* expression and remove the sites dependent only on plant genotypes, we performed *t*-test between time points 0 and 1 h, and 0 and 3 h, after Dex treatment in each genotype ($P \leq 0.05$). We found that 111 unique sites were significantly differentially phosphorylated after Dex treatment at 1 or 3 h in *Dex:avrRpt2*. Twelve sites were highly phosphorylated after Dex treatment in both lines, but only two of these phosphorylation sites (S280 and S283 of PIP2B) were phosphorylated to a similar degree in both lines, suggesting that, for these sites, the increased phosphorylation at these two sites is caused by *avrRpt2* expression or Dex treatment independently on RPS2 and AvrRpt2. The other 10 sites were phosphorylated in *rpm1rps2/Dex:avrRpt2*, but the ratio increase was at least two-fold greater in *Dex:avrRpt2*. These data suggest that, although phosphorylation at these 10 sites can potentially also be induced by AvrRpt2 or Dex application alone, phosphorylation of these sites is significantly enhanced on RPS2 activation (Table S1). In summary, we identified 109 sites differentially phosphorylated upon activation of RPS2. Of these 109 sites, 84 sites were increased in phosphorylation (Fig. 2a; Table S2) and 25 sites were decreased in phosphorylation (Fig. 2b; Table S3). Hereafter, we call these sites 'RPS2-regulated phosphorylation sites'. The majority of the upregulated phosphorylation sites are statistically significantly phosphorylated at 3 h after Dex spray, whereas the majority of downregulated phosphorylation sites are dephosphorylated at 1 h after Dex spray. We also investigated the identified phosphosites for MAPK and CALCIUM-DEPENDENT PROTEIN KINASE (CPK) phosphorylation motifs. We found that 32 and 10 phosphosites of 84 RPS2-upregulated phosphosites contain MAPK and CPK phosphorylation motifs, respectively (Table S2).

Changes in the phosphorylation intensities on proteins could potentially also be explained by alterations in protein abundance or a change in protein localization. Therefore, we also analyzed total protein abundance in nonphosphopeptide-enriched fractions of the samples (Tables S1–S3). These data revealed that the changes in abundance of some phosphorylation sites could be attributed to the changes in protein abundance at the membrane. We could not detect all proteins for which phosphorylated residues were quantified, potentially because of the low abundance of these proteins. Consequently, changes in phosphorylation intensities of such low-abundance proteins could be the result of changes in protein abundance at the membrane with a similar level of phosphorylation after *AvrRpt2* expression, changes in phosphorylation status after *AvrRpt2* expression, or both.

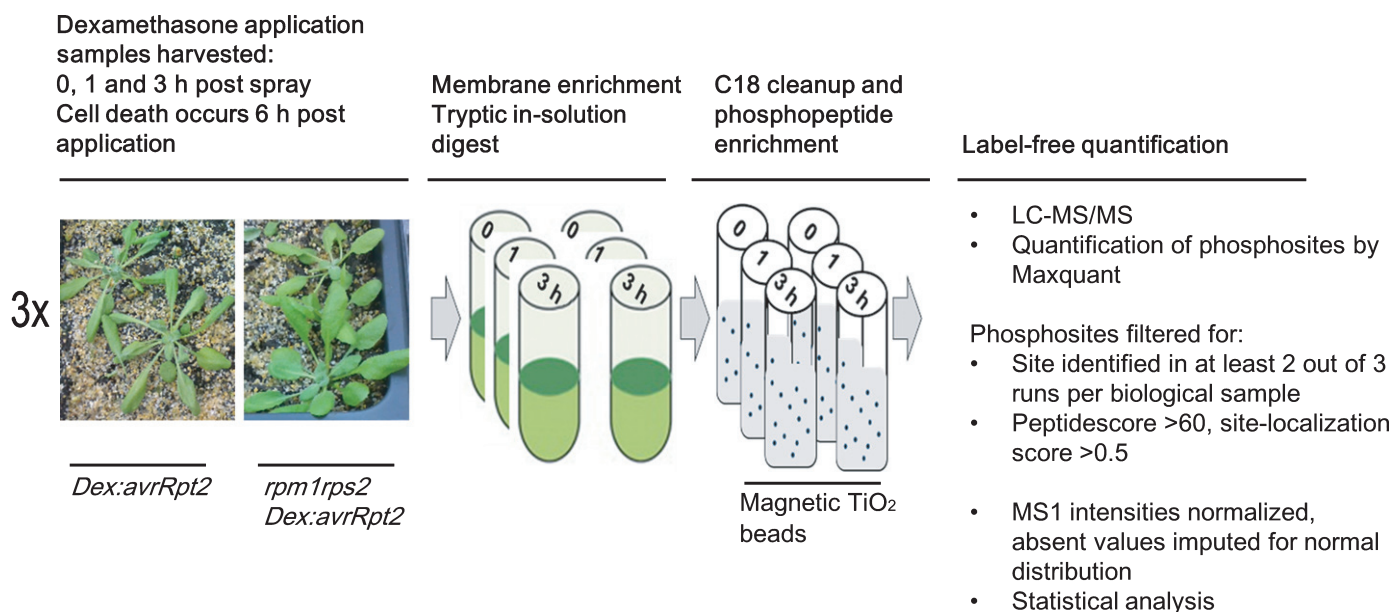


Fig. 1 Schematic representation of the large-scale phosphoscreen. Individual steps are highlighted and annotated. For further details, see the experimental procedures in the Materials and Methods section.

Of note, even for the abundant proteins whose protein levels were detectable in the nonphosphopeptide-enriched samples, we could not fully exclude the possibility that a decrease in phosphorylation would be caused by selective degradation and/or altered localization of the phosphorylated protein.

Overlap in RPS2- and FLS2-induced phosphorylation sites

We found that 14 of 109 RPS2-regulated phosphorylation sites overlapped with previously identified flg22/FLS2-regulated phosphorylation sites (the phosphorylation at 11 sites was increased and that at three sites was decreased during both ETI and PTI) (Table 1). As our phosphoproteomic strategy is not fully identical in approach to previous studies aimed at the identification of PAMP-regulated phosphorylation sites (Benschop *et al.*, 2007; Nühse *et al.*, 2007), there may, in fact, be more overlap in phosphorylation sites regulated during both ETI and PTI. Examples of such overlapping sites are the phosphorylation sites in RBOHD, the ABC-transporter PENETRATION-3 (PEN3), the plasma membrane-localized calcium-ATPase AUTOINHIBITED Ca²⁺ ATPASE-8 (ACA8) and the non-canonical G α protein EXTRA-LARGE GTP-BINDING PROTEIN-2 (XLG2) (Benschop *et al.*, 2007; Nühse *et al.*, 2007; Tables 1, S4). For most of these sites, total protein levels did not change significantly during RPS2 activation (Tables 1, S4). Below, we discuss these proteins in more detail.

RPS2 signaling strongly induced RBOHD phosphorylation at residues S163, S343 and S347 (Fig. 2; Table 1). We also found induced phosphorylation at S33. However, care must be taken for this site, because RBOHD protein amounts increased to a similar extent as S33 phosphorylation upon RPS2 activation (Table S4). Treatment with flg22, elf18 or chitin induces RBOHD phosphorylation at residues S163, S343 and S347, and these phosphorylated residues are required for full ROS

production on PTI (Dubielis *et al.*, 2013; Kadota *et al.*, 2014; Li *et al.*, 2014). In particular, BIK1 phosphorylates RBOHD residues S343 and S347, and CPKs phosphorylate RBOHD residues S163 and, possibly, S347 during PTI. Recently, it was found that the MAP4K SIK1 is also involved in the full phosphorylation on S339 and S347 during PTI (M. Zhang *et al.*, 2018).

PEN3 is involved in nonhost resistance against the powdery mildew fungus *Blumeria graminis* f. sp. *hordei* (*Bgh*), but also has broader roles in resistance, including ETI signaling (Johansson *et al.*, 2014). PEN3 delivers indole glucosinolates to the apoplast at the plasma membrane (Kwon *et al.*, 2008). In addition, the *pen3* mutant shows defects in cell death induction by avirulent bacteria, such as *Pto* DC3000 (*avrRpm1*) and *Pto* DC3000 (*avrRps4*), and an avirulent isolate of the oomycete *Hyaloperonospora arabidopsis* (*Hpa*) (Piasecka *et al.*, 2015). We found that RPS2 signaling induced phosphorylation of PEN3 at S40 and S45, which are also reported as flg22/FLS2-inducible phosphorylation sites (Tables 1, S4). Moreover, these sites have been shown recently to be required for the function of PEN3 in immunity against *Bgh* (Underwood & Somerville, 2017). These results suggest that PEN3 is activated during both PTI and ETI by phosphorylation at common residues, which may be required for the transport of indole glucosinolates or other antimicrobials to restrict pathogen colonization.

ACA8 forms a protein complex with FLS2 and is involved in flg22-inducible Ca²⁺ signaling (Frei dit Frey *et al.*, 2012). flg22 treatment/perception induces phosphorylation at ACA8 S22, and this N-terminal phosphorylation is important for the interaction of ACA8 with CALMODULIN (CaM), leading to ACA8 activation (Giacometti *et al.*, 2012). We found that RPS2 activation similarly induced S22 phosphorylation (Tables 1, S4), suggesting CaM-mediated activation of ACA8 during both PTI and ETI. Interestingly, CPK16 can phosphorylate S22 of ACA8 *in vitro* (Giacometti *et al.*, 2012), suggesting a role of CPK16 in

(a) Upregulated phosphorylation sites by AvrRpt2/RPS2

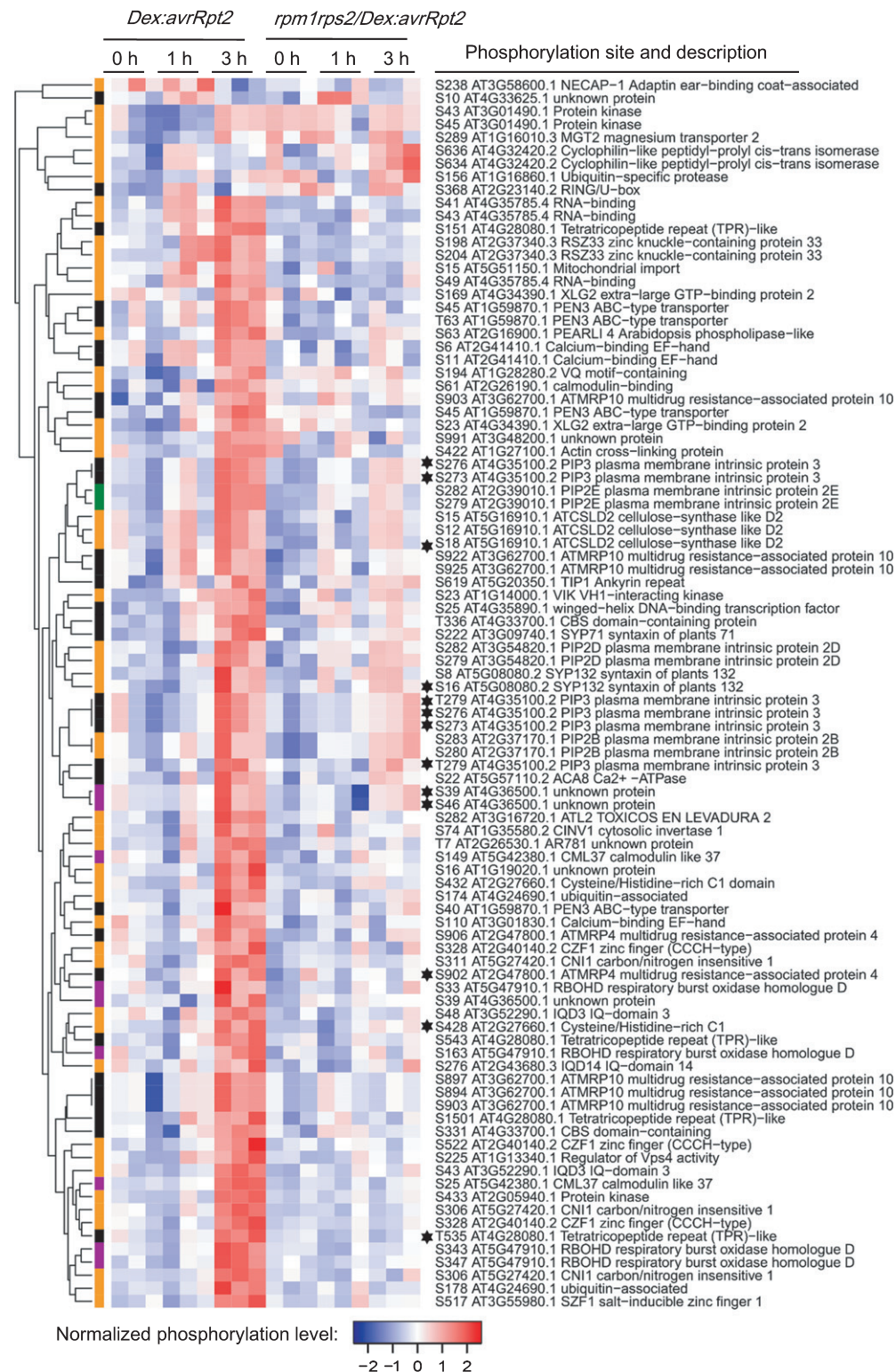


Fig. 2 Heat-maps showing RESISTANT TO *P. SYRINGAE*-2 (RPS2)-regulated phosphorylation sites. The phosphorylation sites shown are differentially phosphorylated on RPS2 activation (one-way ANOVA $P \leq 0.05 + t$ -test $P \leq 0.05$). (a) Phosphorylation sites significantly upregulated by RPS2 in *Dex:avrRpt2* plants. (b) Phosphorylation sites significantly downregulated by RPS2 in *Dex:avrRpt2* plants. Dendrograms were obtained by hierarchical clustering to represent Euclidian distances of normalized expression profiles. The colored sidebar indicates the regulation at the protein level in total protein membrane fractions (Supporting Information Table S1): black, sites for which the protein levels were not significantly altered amongst treatments; magenta, sites for which protein levels were significantly increased in *Dex:avrRpt2* plants on application of dexamethasone (Dex); green, sites for which protein levels were significantly decreased in *rpm1rps2/Dex:avrRpt2* plants on Dex application; orange, sites for which no peptides were detected in total protein samples; black stars, the phosphorylation sites upregulated in both lines after Dex treatment.

(b) Downregulated phosphorylation sites by AvrRpt2/RPS2

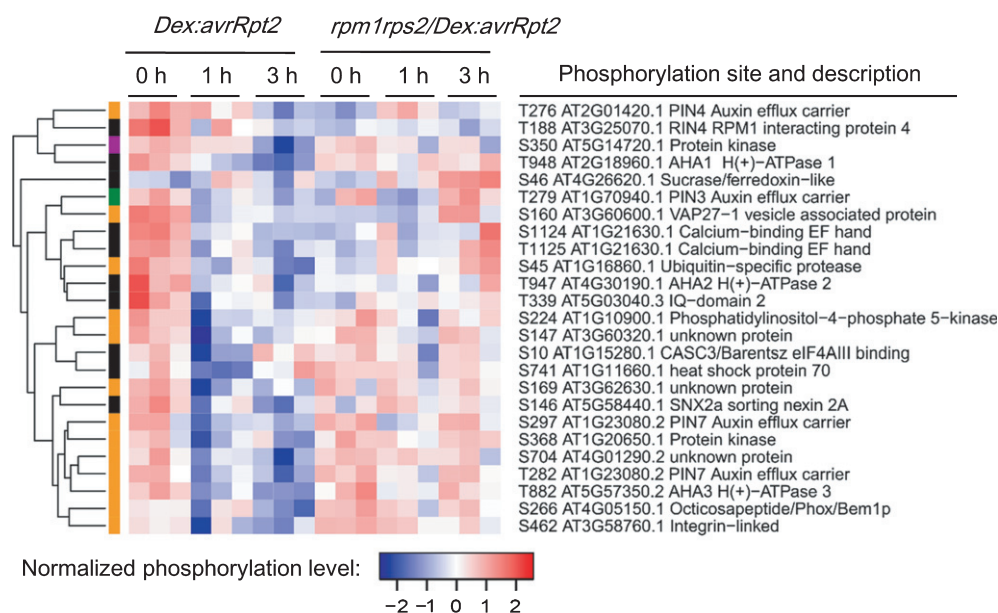


Fig. 2 Continued.

Table 1 Common residues differentially phosphorylated on activation of RPS2 and flg22 treatment.

	ETI (<i>AvrRpt2</i> expression by Dex treatment)				PTI (flg22 treatment)	CPK or MAPK phosphorylation motif
	Ratio Dex 3 h/0 h in <i>Dex:avrRpt2</i>		Ratio Dex 3 h/0 h in <i>rpm1rps2/Dex:avrRpt2</i>			
	Phosphorylation	Protein level	Protein level	Phosphorylation	Ratio flg22/mock Phosphorylation	
RBOHD (AT5G47910)	S163 10.97 S343 13.08 S347 13.83	3.32	1.39 0.83 0.94	1.28	3.72 ¹ 4.7 ¹ , 20.69 ^{2,4} 3.5 ¹ , 20.69 ^{2,4}	
PEN3 (AT1G59870)	S40 6.87 S45 27.23 ⁵ , 12.85 ⁶	1.44	0.86 0.18 ⁵ , 1.34 ⁶	0.98	8.21 ² 4.66 ²	φ-X-X-X-X-S/T-X-B ⁷ φ-X-X-X-X-S/T-X-B ⁷
ACA8 (AT5G57110)	S22 20.80	1.50	2.48	0.68	3.74 ²	φ-X-X-X-X-S/T-X-B ⁷
XLG2 (AT4G34390)	S23 13.23 S169 3.02	nd	0.32 0.20	nd	Not quantified ³ Not quantified ³	
CBS domain-containing protein (AT4G33700)	S331 5.65 T336 5.96	1.11	1.07 0.70	0.66	1.8 ¹ 2.9 ¹	S/T-P ⁸ S/T-P ⁸
PEARL1 4 (AT2G16900)	S63 9.95	nd	1.33	nd	4.2 ¹	S/T-P ⁸
AHA1 (AT2G18960)	T948 0.10	1.06	0.78	0.90	0.33 ²	
AHA2 (AT4G30190)	T947 0.22	1.07	0.97	0.92	0.42 ²	
AHA3 (AT5G57350)	T882 0.22	nd	0.60	nd	0.38 ²	

CPK, CALCIUM-DEPENDENT PROTEIN KINASE; Dex, dexamethasone; ETI, effector-triggered immunity; MAPK, mitogen-activated protein kinase; PTI, pathogen-associated molecular pattern (PAMP)-triggered immunity.

Phosphorylation data after flg22 treatment were extracted from the articles indicated. The data are shown as the fold change. For the data of RPS2, the fold change of the phosphorylated sites was calculated based on raw intensities. The fold change of the protein levels was calculated based on the Maxquant label-free quantification intensities transformed to raw intensities (see Supporting Information Methods S1). Significantly differentially phosphorylated sites with a ratio higher than 1.5 or lower than 0.5 were kept; see also Tables S1–S3.

¹The phosphorylation ratio at 10 min after flg22 treatment (Benschop *et al.*, 2007).

²The best phosphorylation ratio at 7 min after flg22 treatment of five replicates is shown (Nühse *et al.*, 2007).

³Phosphorylated but not quantified (Liang *et al.*, 2016).

⁴Double phosphorylated peptide.

⁵Calculated based on singly phosphorylated phosphopeptide intensities (Table S1 Multiplicity = __1).

⁶Calculated based on doubly phosphorylated phosphopeptide intensities (Table S1 Multiplicity = __2).

⁷CPK phosphorylation motif: φ-X-X-X-X-S/T-X-B (S/T is the phosphorylated residue, B is a basic residue, φ is a hydrophobic residue, X is any residue) (Huang & Huber, 2001; Huang *et al.*, 2001; Hernandez Sebastia *et al.*, 2004).

⁸MAPK phosphorylation motif S/T-P (S/T is the phosphorylated residue).

nd, not detected.

the PTI and ETI signaling pathways. CBL-INTERACTING PROTEIN KINASE-9 (CIPK9) in a complex with the plasma membrane Ca^{2+} sensor CALCINEURIN B-LIKE PROTEIN-1 (CBL1) phosphorylates ACA8, thereby regulating its activity (Costa *et al.*, 2017). However, the role of ACA8, as well as CPK16, CIPK9 and CBL1, during ETI remains to be elucidated.

XLG2 is a member of the heterotrimeric G proteins and participates in signaling with the $\text{G}\beta$ protein GTP-BINDING PROTEIN BETA-1 (AGB1), and the $\text{G}\gamma$ proteins G PROTEIN GAMMA-SUBUNIT-1 (AGG1) and AGG2 (Zhu *et al.*, 2009; Chakravorty *et al.*, 2015). We found an increase in S23 and S169 phosphorylation of XLG2 after activation of RPS2, but we could not detect XLG2 total protein in the nonphosphopeptide-enriched fractions (Table 1). XLG2 interacts with FLS2 and BIK1, and functions to attenuate the proteasome-mediated degradation of BIK1 (Liang *et al.*, 2016; Wang *et al.*, 2018). After *flg22* recognition, XLG2 is phosphorylated by BIK1, dissociates from AGB1 and the phosphorylated XLG2 enhances ROS production, possibly through the modulation of RBOHD (Liang *et al.*, 2016; Wang *et al.*, 2018). Multiple sites of XLG2, including S23 and S169, are phosphorylated in *flg22*-treated protoplast cells (Liang *et al.*, 2016), suggesting that these are common phosphorylation sites during both PTI and ETI. Although the roles of these phosphorylation sites need to be elucidated further, our results suggest that XLG2 phosphorylation may also contribute to RBOHD-mediated ROS production during ETI.

RPS2 and FLS2 activation results in dephosphorylation of H^{+} -ATPases

Plasma membrane H^{+} -ATPases (AHAs) generate the proton-motive force across the plasma membrane necessary to activate ion and metabolite transport (Morsomme & Boutry, 2000). AHAs also play a pivotal role in the opening of stomata, which are important entry sites for bacteria during natural infection (Yamauchi *et al.*, 2016). We found that RPS2 activation resulted in C-terminal dephosphorylation of AHA1 at T948 and at homologous sites of AHA2 (T947) and AHA4 (T955) (Figs 2, S2a; Tables 1, S4). Interestingly, FLS2 activation similarly induces dephosphorylation of AHA1 at T948 and AHA2 at T947 (Nühse *et al.*, 2007).

RPS2 regulates changes in phosphorylation status of defense-associated proteins

In addition to the overlapping PTI and ETI phosphorylation sites, we discovered a set of novel sites involved in RPS2 signaling on a variety of proteins, including defense-associated proteins. These sites are on proteins such as the kinase RIPK and PLASMA MEMBRANE INTRINSIC PROTEIN (PIP) aquaporins (Fig. 2; Table S2).

Currently, the involvement of RIPK in the RPS2 signaling pathway is unknown (Liu *et al.*, 2011). However, we found that RPS2 activation induced dramatic phosphorylation of RIPK at the residue S433 (Fig. 2; Table S2). The importance of RIPK

phosphorylation during RPS2-mediated ETI requires future investigation as we did not detect RIPK total protein in the non-phosphopeptide-enriched fractions (Table S1).

PIP aquaporins can transport water and H_2O_2 between the apoplast and cytoplasm. C-terminal PIP phosphosites are strongly conserved among PIPs and required for their activation (Maurel *et al.*, 2015). *Arabidopsis* PIP1E transports apoplastic H_2O_2 produced by RBOH after PAMP treatment to the cytoplasm (Tian *et al.*, 2016). This transport is required for the full activation of immune responses, including pathogenesis-related gene expression and callose deposition. PIP2A is also required for the intracellular accumulation of H_2O_2 , as well as stomatal closure, induced by PAMPs (Rodrigues *et al.*, 2017). We found that several conserved residues at the C-terminal region of PIPs, such as S279 and S282 of PIP2D and PIP2E, and S273, S276 and S279 of PIP3, were highly phosphorylated on *avrRpt2* expression in the presence of RPS2 (Figs 2, S2b; Table S4). PIPs may be activated during ETI and transport both water and H_2O_2 to the cytoplasm in a similar manner as during PTI. Recently, the importance of an aqueous apoplast for successful bacterial proliferation was shown (Xin *et al.*, 2016). In line with our results, *AvrRpt2*-induced ETI failed to induce water soaking (Xin *et al.*, 2016). It is tempting to speculate that the activation of PIPs contributes to reducing the aqueous space in the apoplast, thereby suppressing bacterial growth.

In addition to the upregulated phosphorylations, the activation of RPS2 resulted in dephosphorylation of the auxin transporter PIN-FORMED-3 (PIN3) at T279 and, possibly, PIN4 at T276 and PIN7 at T282, reflecting a possible crosstalk of ETI signaling and auxin signaling (Figs 2, S2c; Table S3). Interestingly, *AvrRpt2* promotes the virulence of *Pto* DC3000 by stimulating the turnover of key auxin transcription repressors Aux/IAA, thereby activating auxin responses (Cui *et al.*, 2013). Although the role of the phosphorylation of these PIN residues needs to be elucidated further, RPS2-mediated dephosphorylation of PINs may change the localization of these auxin transporters, thereby altering auxin transport to suppress *AvrRpt2*-induced auxin signaling (Lofke *et al.*, 2013).

Interestingly, we also found *AvrRpt2* itself to be phosphorylated at S97. However, we only observed S97 phosphorylation in the absence of the RPM1 and RPS2 receptors (Fig. 2; Table S1). This suggests a possible involvement of *AvrRpt2* phosphorylation for its virulent function, and suppression of *AvrRpt2* phosphorylation during ETI signaling. However, we could not correlate this phosphorylation to *AvrRpt2* protein levels, as we did not detect *AvrRpt2* protein in unenriched protein samples by MS (Table S1). Instead, we detected a similar *avrRpt2* gene expression pattern by semi-quantitative PCR (Fig. S1b).

Phosphorylation of common RBOHD residues is required for ROS production during ETI

We hypothesize that the common PTI and ETI phosphorylation targets are potential convergent points of immune signaling and should therefore tightly regulate the activity of such proteins. As RBOHD contains several such common phosphosites, we sought

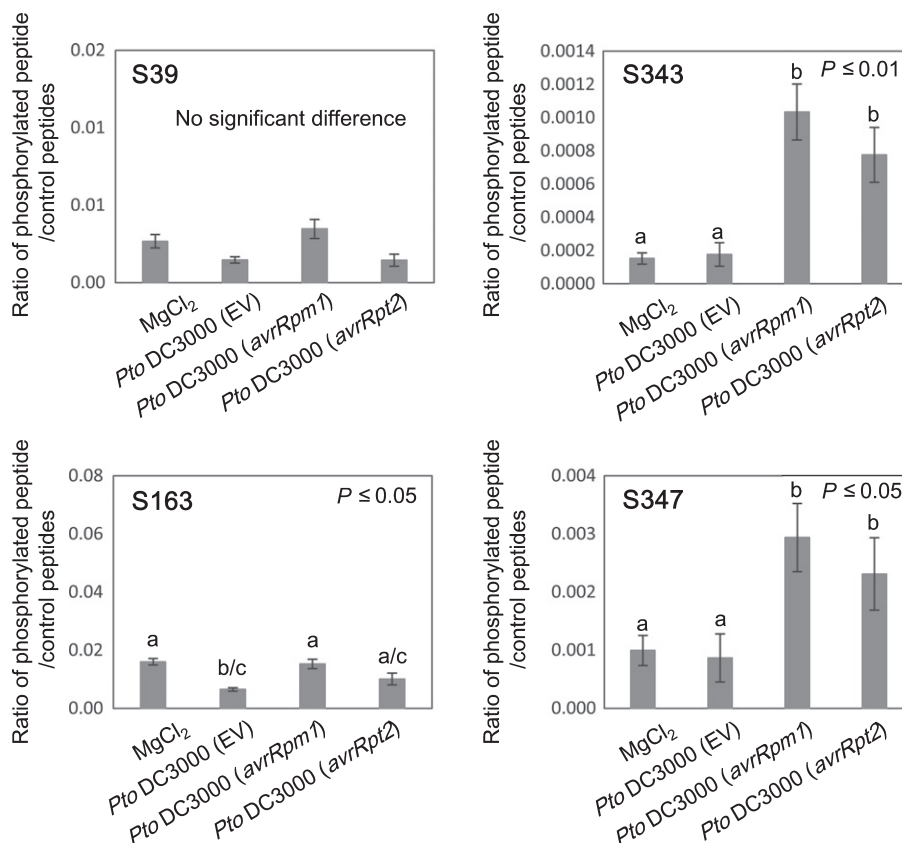


Fig. 3 Avirulent bacteria induce phosphorylation of RESPIRATORY BURST OXIDASE HOMOLOG D (RBOHD) at specific residues. Selected reaction monitoring (SRM) analysis of the phosphorylation sites 6 h after infiltration with 10 mM MgCl₂ solution, *Pseudomonas syringae* pv *tomato* (*Pto*) DC3000 EV (empty vector), *Pto* DC3000 (*avrRpm1*) or *Pto* DC3000 (*avrRpt2*) using a triple quadrupole mass spectrometer. Values are means \pm SE of three biological replicates. Different letters indicate significantly different values at $P \leq 0.05$ for S163 and S347, or at $P \leq 0.01$ for S343 (one-way ANOVA, Tukey *post hoc* test).

to clarify the importance of these common RBOHD sites during PTI and ETI. To confirm that RBOHD phosphorylation during ETI identified in our large-scale screen also occurs on bacterial infection, we syringe inoculated leaves of *rbobD* plants, complemented with *35S:FLAG-RBOHD*, with *Pto* DC3000 EV (empty vector), *Pto* DC3000 (*avrRpm1*), *Pto* DC3000 (*avrRpt2*) or 10 mM MgCl₂ solution. We collected the leaves at 6 h after inoculation, because avirulent effector-mediated transcriptional changes are most highly induced at 6 h after infiltration with *Pto* DC3000 (*avrRpm1*) and *Pto* DC3000 (*avrRpt2*) (Mine *et al.*, 2018), and ROS are also actively produced at this time point (Torres *et al.*, 2002). After collecting the infiltrated leaves, FLAG-RBOHD protein was immunopurified and individual RBOHD phosphorylation sites were quantified by SRM MS on a triple quadrupole mass spectrometer. Both avirulent strains, *Pto* DC3000 (*avrRpm1*) and *Pto* DC3000 (*avrRpt2*), but not virulent *Pto* DC3000 EV or 10 mM MgCl₂ solution, induced phosphorylation at residues S343 and S347 (Fig. 3). By contrast with our large-scale phosphoscreen, residue S163 was not highly phosphorylated 6 h after bacterial infection, suggesting that S163 phosphorylation may be transient on bacterial infection. In addition, the phosphorylation at residue S39, which is a BIK1-dependent flg22-induced RBOHD phosphorylation site (Kadota *et al.*,

2014; Li *et al.*, 2014), was not detectable after infection with any of the bacteria under the conditions tested.

To investigate the role of RBOHD phosphorylation sites S343 and S347 on ROS production during ETI, we generated transgenic *Arabidopsis rbobd* mutant lines expressing either the wild-type (WT) or the S343A/S347A variant of FLAG-tagged RBOHD driven by its endogenous promoter. Both lines expressed comparable amounts of RBOHD protein (Fig. 4a) and did not exhibit any obvious morphological growth phenotypes (Fig. S3a). Interestingly, S343A/S347A plants lost the ability to induce ROS production after infiltration with avirulent *Pto* DC3000 (*avrRpm1*) or *Pto* DC3000 (*avrRpt2*), whereas WT plants induced a strong H₂O₂ accumulation (Fig. 4b). Moreover, the S343A/S347A plants did not show ROS production on flg22 treatment (Fig. S3b) (Nühse *et al.*, 2007). These results demonstrate that S343 and S347 are required for ROS production during both PTI and ETI. Importantly, S343 and S347 are highly conserved in RBOHD homologs amongst different plants (Fig. S4), as well as in most *Arabidopsis* RBOHDs (Kadota *et al.*, 2014). Furthermore, S318 and S322 of RBOHC (corresponding to S343 and S347 in RBOHD) are required for ROS production and root hair formation (Takeda *et al.*, 2008). Together, these results support the idea that these phosphorylation sites play

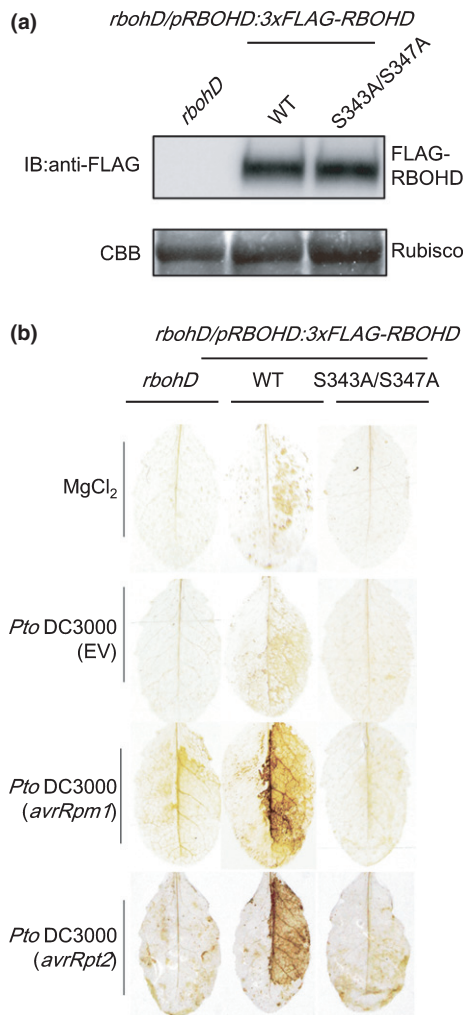


Fig. 4 RESPIRATORY BURST OXIDASE HOMOLOG D (RBOHD) phosphorylation sites S343 and S347 are required for reactive oxygen species (ROS) production during effector-triggered immunity (ETI). (a) Immunoblot showing similar protein levels of FLAG-tagged RBOHD protein in *rbohD* mutants expressing *3xFLAG-RBOHD* wild-type (WT) and the S343A/S347A variant. Coomassie Brilliant Blue G-250 (CBB) stain shows Rubisco protein to demonstrate equal loading. (b) 3,3'-Diaminobenzidine (DAB)-mediated H₂O₂ staining in *rbohD* and *rbohD* mutants expressing *3xFLAG-RBOHD* WT and the S343A/S347A variant 8 h after infiltration with the bacteria. The right halves of the leaves were infiltrated with 10 mM MgCl₂ solution, *Pseudomonas syringae* pv *tomato* (*Pto*) DC3000 EV, *Pto* DC3000 (*avrRpm1*) or *Pto* DC3000 (*avrRpt2*). We repeated the experiment three times with similar results (four to five leaves per genotype were stained each time).

crucial roles in the regulation of RBOHs in various signaling pathways.

BIK1 phosphorylates both S343 and S347 of RBOHD during PTI, and the *bik1* knockout mutant exhibits reduced S343/S347 phosphorylation and PTI-mediated ROS burst (Kadota *et al.*, 2014; Li *et al.*, 2014). Therefore, we investigated the involvement of BIK1 in ROS production during ETI. We found that BIK1 protein accumulated on infection with *Pto* DC3000 (*avrRpm1*) and, to a lesser extent, *Pto* DC3000 EV (Fig. 5a). PBS1-LIKE-1 (PBL1) is a kinase functionally redundant with BIK1, and a

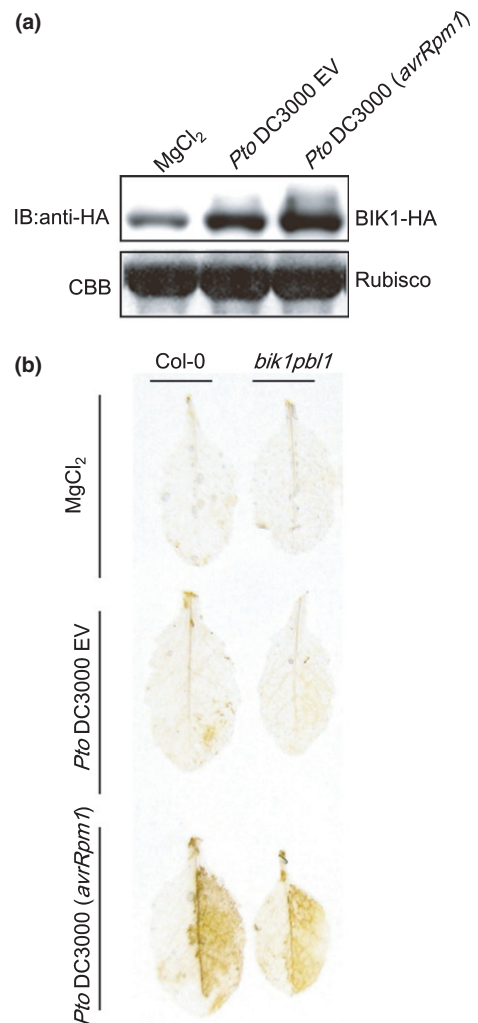


Fig. 5 The *bik1pbl1* double mutant does not exhibit a defect in reactive oxygen species (ROS) accumulation during effector-triggered immunity (ETI). (a) BOTRYTIS-INDUCED KINASE-1 (BIK1) protein accumulates after infection with *Pseudomonas syringae* pv *tomato* (*Pto*) DC3000 (*avrRpm1*). *pBIK1:BIK1-HA* plants were inoculated with 5 mM MgCl₂, *Pto* DC3000 empty vector (EV) or *Pto* DC3000 (*avrRpm1*) (2.5×10^7 cfu (colony-forming units) ml⁻¹) and BIK1-HA protein amount was determined by immunoblot analyses using anti-HA antibody. Coomassie Brilliant Blue G-250 (CBB) stain shows Rubisco protein to demonstrate equal loading. (b) H₂O₂ accumulation in Col-0 and *bik1pbl1* mutant after inoculation with 10 mM MgCl₂, *Pto* DC3000 EV or *Pto* DC3000 (*avrRpm1*) (2.5×10^7 cfu ml⁻¹). H₂O₂ accumulation was detected by 3,3'-diaminobenzidine (DAB). The experiments were performed three times with similar results.

bik1pbl1 double mutant shows less PAMP-inducible ROS production and RBOHD phosphorylation (J. Zhang *et al.*, 2010; Kadota *et al.*, 2014; Li *et al.*, 2014). However, *bik1pbl1* double mutants induced H₂O₂ accumulation similar to Col-0 on infection with *Pto* DC3000 (*avrRpm1*) (Fig. 5b), suggesting that BIK1 may not play a major role in RBOHD phosphorylation during ETI. This is consistent with the fact that RPS2 activation did not induce significant phosphorylation at other BIK1-mediated phosphorylation sites, such as S39 and S339, suggesting that other kinases may phosphorylate RBOHD at S343 and S347 during RPS2-mediated ETI.

The autoimmunity phenotype of *rbohD* and semi-dwarf phenotype of *rbohDrbohF* can be complemented with the RBOHD S343A/S347A variant

In addition to a direct toxic effect of ROS to microbial pathogens, the RBOHD-induced ROS burst plays critical roles in immunity, including stomatal closure, which hampers the entrance of pathogens through these pores, callose deposition, which prevents pathogen invasion, and long-distance immune signaling, which induces resistance against secondary infections (Suzuki *et al.*, 2011; Kadota *et al.*, 2015). However, the role of RBOHD-mediated ROS in resistance against avirulent pathogens is still unclear, mostly because of a lack of genetic evidence. *rbohD* mutants do not produce ROS on infection with avirulent *Pto* strains and an avirulent *Hpa* isolate Emco5 (Torres *et al.*, 2002; Gao *et al.*, 2013). However, the *rbohD* and *rbohDrbohF* double mutants (RBOHF is functionally redundant with RBOHD in many immune responses) are resistant to virulent and avirulent pathogens as a result of the constitutive or inducible activation of immune responses (Torres *et al.*, 2002; Marino *et al.*, 2012). Notably, *rbohD* plants hyperaccumulate salicylic acid, ethylene, the antimicrobial compound scopoletin and *PR-1* gene transcripts on pathogen challenge (Pogany *et al.*, 2009; Chaouch *et al.*, 2012; Kadota *et al.*, 2014). Indeed, we observed that *rbohD* mutants expressed higher amount of transcripts of *FERULOYL COA ORTHO-HYDROXYLASE 1* (*F6'H1*), a key enzyme for scopoletin biosynthesis, after infection with *Pto* DC3000 (*avrRpt2*) (Fig. 6a). Interestingly, however, this phenotype was suppressed in *rbohD* plants expressing the WT or S343A/S347A RBOHD variant, suggesting that the overactivation of immunity in the null *rbohD* mutant may compensate for the loss of ROS-based immunity. Notably, similar constitutive or overactivation of immunity was seen in null mutants of other positive regulators of immune signaling, such as BAK1, BIK1, POWDERY MILDEW RESISTANT-4 (PMR4) and MITOGEN-ACTIVATED PROTEIN KINASE-4 (MPK4) (Petersen *et al.*, 2000; Nishimura *et al.*, 2003; He *et al.*, 2007;

Kemmerling *et al.*, 2007; J. Zhang *et al.*, 2010; Z. Zhang *et al.*, 2012, 2017). A possible explanation is that these components are guarded by NLR proteins, as seen for MPK4 (Z. Zhang *et al.*, 2012), whose kinase activity on CALMODULIN-BINDING RECEPTOR-LIKE CYTOPLASMIC KINASE 3 (CRCK3) is monitored by NLR protein SUMM2 (Lolle *et al.*, 2017; Z. Zhang *et al.*, 2017).

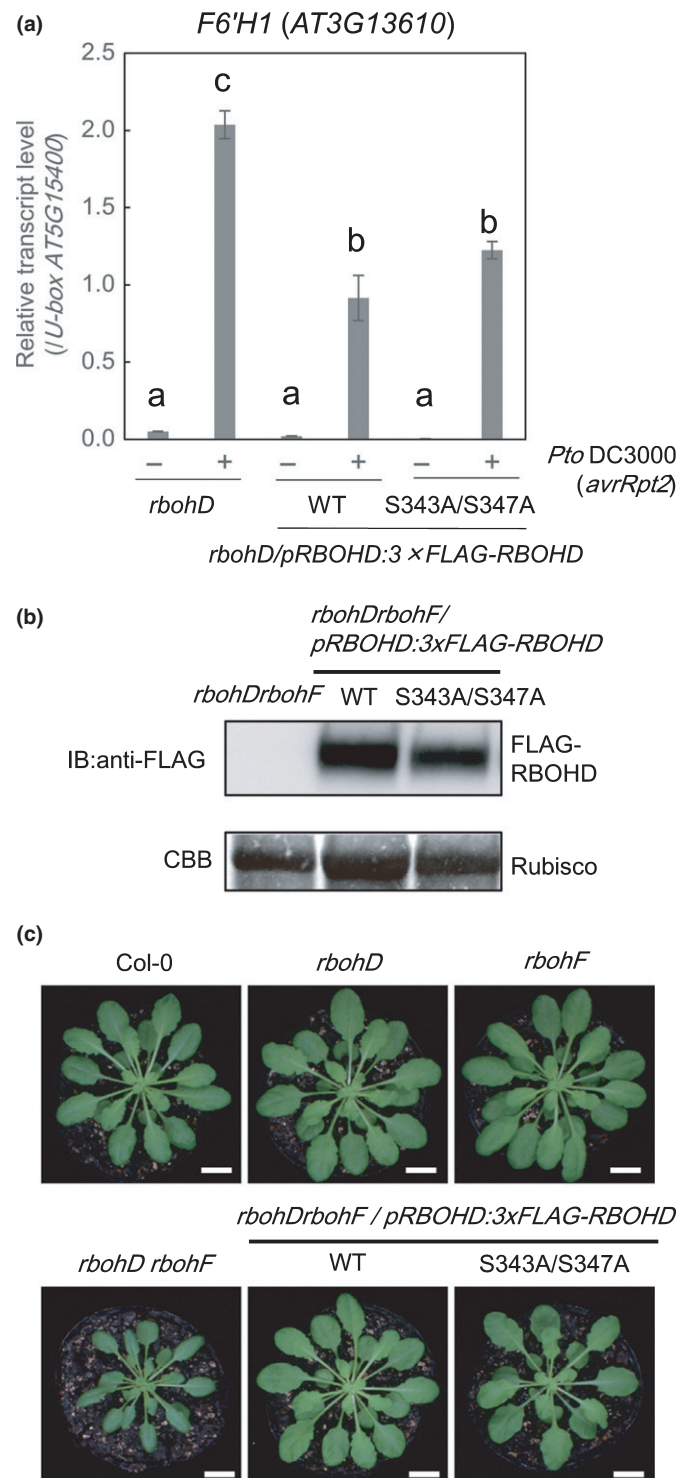


Fig. 6 RBOHD-S343A/S347A variant can complement the overactivation of immune-related gene expression in *rbohD* and the semi-dwarf autoimmunity phenotype of *rbohDrbohF*. (a) Loss of RESPIRATORY BURST OXIDASE HOMOLOG D (RBOHD) leads to increased expression of *FERULOYL COA ORTHO-HYDROXYLASE 1* (*F6'H1*) on bacterial perception. Gene expression of *F6'H1* in leaves infiltrated with *Pseudomonas syringae* pv *tomato* DC3000 (*avrRpt2*) (2.5×10^7 cfu (colony-forming units) ml^{-1}) or 10 mM MgCl_2 solution for 24 h was measured by quantitative PCR analysis. The relative transcript levels were calculated by normalization to the *U-box* housekeeping gene transcript (*At5g15400*). Data are the mean \pm SE of three technical replicates. Different letters indicate significantly different values at $P \leq 0.05$ (one-way ANOVA, Tukey *post hoc* test). The experiments were performed three times with similar results. (b) Immunoblot showing equal FLAG-RBOHD protein level in leaves of *rbohDrbohF/pRBOHD:3xFLAG-RBOHD* (wild-type, WT) and *rbohDrbohF/pRBOHD:3xFLAG-RBOHD* (S343A/S347A) lines. Leaf tissue of the *rbohDrbohF* double mutant was used as negative control. Coomassie Brilliant Blue G-250 (CBB) shows Rubisco protein to demonstrate equal loading. (c) Growth phenotypes of 6-wk-old plants. Bars, 1 cm.

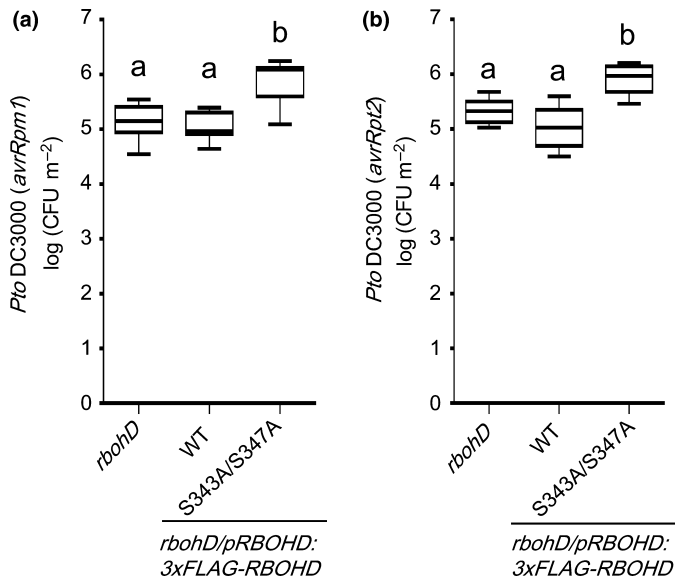


Fig. 7 RESPIRATORY BURST OXIDASE HOMOLOG D (RBOHD) phosphorylation sites S343 and S347 are required for effector-triggered immunity (ETI). Bacterial growth of *Pseudomonas syringae* pv *tomato* (*Pto*) DC3000 (*avrRpm1*) (a) and *Pto* DC3000 (*avrRpt2*) (b) in *rbohD* and *rbohD* expressing 3xFLAG-RBOHD wild-type (WT) or the S343A/S347A variant. Bacteria were syringe infiltrated in three leaves per plant at a concentration of 1×10^5 cfu (colony-forming units) ml^{-1} . At 3 d post-infiltration, the leaves were harvested to determine bacterial growth. Data are the means \pm SD of eight replicates. Solid horizontal lines within the boxes show the median. Different letters indicate significantly different values at $P \leq 0.01$ (one-way ANOVA, Tukey *post hoc* test). These experiments were repeated three times with similar results.

Although the *rbohD* mutant does not show obvious phenotypes under standard growth conditions, the *rbohDrbohF* double mutant is semi-dwarf and shows a strong autoimmune phenotype, including the development of necrotic lesions and callose deposition in mature leaves (Torres *et al.*, 2002). To determine whether S343 or S347 phosphorylation plays a role in this phenotype, we generated *rbohDrbohF* mutant lines expressing the WT or the S343A/S347A variant of RBOHD at similar levels (Fig. 6b). Remarkably, the semi-dwarf phenotype of the *rbohDrbohF* double mutant was recovered by the expression of WT, as well as the expression of the S343A/S347A RBOHD variant (Fig. 6c), showing that the presence of RBOHD protein, but not phosphorylation at S343 or S347, is required for the normal growth and suppression of autoimmunity in *rbohD* and *rbohDrbohF* mutants (Fig. 6c). These results suggest that the activity of RBOHD is not required for the suppression of autoimmunity and supports a hypothesis in which RBOHD and RBOHF are guarded by one or more NLRs.

RBOHD phosphorylation of S343 or S347 is required for immunity

Although ROS are involved in various immune responses, there is no clear genetic evidence showing the crucial roles of ROS in resistance against avirulent pathogens. As *rbohD* lines expressing the RBOHD S343A/S347A variant do not show any obvious

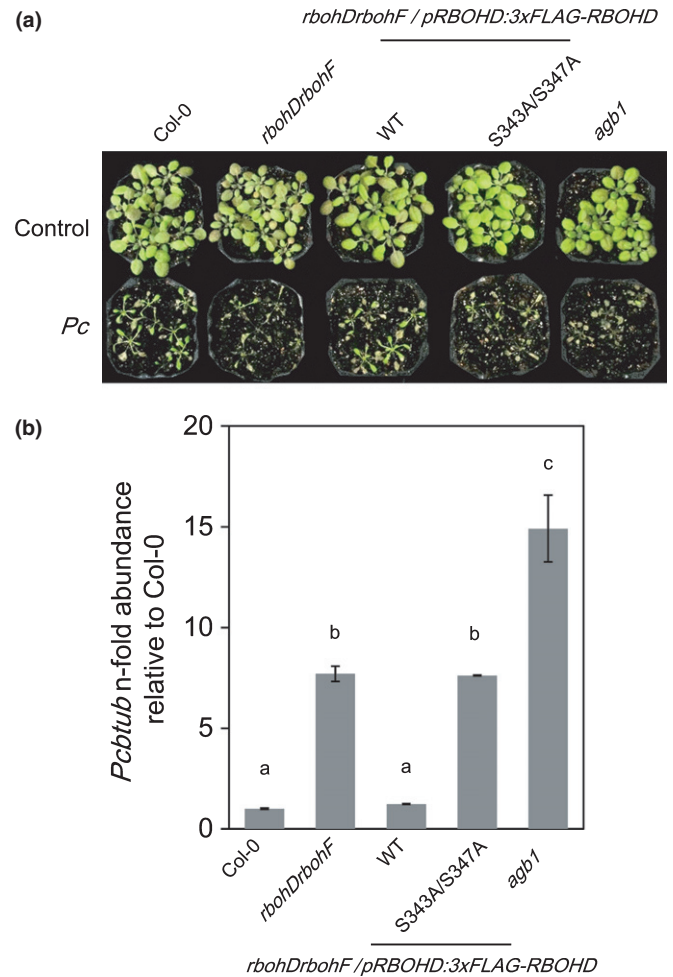


Fig. 8 The double mutant *rbohDrbohF* shows weakened resistance to virulent *Plectosphaerella cucumerina* (*PcBMM* isolate). (a) Symptoms of 18-d-old plants after spray inoculation with *PcBMM* (4×10^6 spores ml^{-1}). WT, wild-type. (b) Quantification of *PcBMM* biomass. Fungal DNA was quantified by quantitative PCR at 6 d post-inoculation (dpi) using specific primers for *PcBMM* β -TUBULIN and normalized to the *Arabidopsis thaliana* UBIQUITIN 10 gene. Bars represent the averages (\pm SE) of fungal DNA levels relative to Col-0 plants from two replicates. Statistical analysis was performed by ANOVA, corrected with Bonferroni *post hoc* test. Different letters indicate significant differences ($P \leq 0.05$). The experiment was repeated twice with similar results.

autoimmune-related phenotypes, we used these lines to study the relevance of S343 and S347 phosphorylation in ETI. *Pto* DC3000 (*avrRpm1*) and *Pto* DC3000 (*avrRpt2*) grew significantly more in the *rbohD* mutant expressing the RBOHD S343A/S347A variant than in the mutant expressing WT RBOHD (Fig. 7), showing that phosphorylation at S343 and S347 is important for resistance against these avirulent bacterial strains.

In addition, we used the *rbohDrbohF* lines with the RBOHD S343A/S347A variant to test the resistance against the necrotrophic fungus *PcBMM*. Both RBOHD and RBOHF are required for resistance against *PcBMM*, as the *rbohDrbohF* mutant was shown to display enhanced susceptibility to *PcBMM* (Torres *et al.*, 2013; Morales *et al.*, 2016). As reported, Col-0 and

WT RBOHD complementation lines were resistant to *PcBMM* (Fig. 8). By contrast, *rbobDrbohF* and RBOHD S343A/S347A plants were significantly more susceptible, similar to the *agb1* mutant (impaired in the G β subunit of the heterotrimeric G protein), which is a susceptible control (Torres *et al.*, 2013) (Fig. 8). These results suggest that the RBOHD residues S343 and S347 contribute to the resistance against *PcBMM*. The *rbobD* single mutants and the corresponding complementation lines were all resistant to *PcBMM* (Fig. S5), indicating that RBOHD has a functional redundancy with RBOHF in immunity against *PcBMM*. The importance of S343 and S347 in the resistance suggests that plants actively phosphorylate RBOHD and produce ROS in response to *PcBMM*, possibly through the recognition of unidentified PAMPs or damage-associated molecular patterns (DAMPs). The result also suggests that the susceptibility of *rbobDrbohF* is probably not a result of the overactivation of the salicylic acid-dependent pathway, which antagonizes jasmonic acid-based resistance against necrotrophic pathogens (Thaler *et al.*, 2012), but of the loss of RBOHD activation and ROS production.

Discussion

RPS2 and FLS2 trigger similar phosphorylation patterns at immune components

Previous studies have shown that similar responses are induced during PTI and ETI, although the dynamics and amplitude differ between the two signaling arms (Dodds & Rathjen, 2010; Tsuda & Katagiri, 2010; Thomma *et al.*, 2011). Our study reveals a common set of differentially phosphorylated sites during both PTI and ETI. Such common sites may be convergent points of both signaling pathways, and phosphorylation or dephosphorylation of such residues probably plays a crucial role in regulating the activity of defense components. In support of this, we found that phosphorylation at specific conserved residues in RBOHD is required for ROS production in both PTI and ETI. In addition, we found commonly phosphorylated sites during PTI and ETI in PEN3 and ACA8. Importantly, previous mutational analyses have shown that these phosphorylation sites of PEN3 and ACA8 are required for their activation (Giacometti *et al.*, 2012; Underwood & Somerville, 2017).

We also found a commonly dephosphorylated site, T948 on AHA1, during PTI and ETI. Phosphorylation at T948 of AHA1 creates a binding site for a 14-3-3 protein, and 14-3-3 interaction alters the orientation of the autoinhibitory C-terminal domain, resulting in AHA1 activation (Svennelid *et al.*, 1999). Thus, dephosphorylation of AHA1 at T948 would cause dissociation of 14-3-3, leading to the inactivation of AHA1. AHA1 inactivation may lead to the inhibition of stomatal opening, thereby preventing bacterial entry (Yamauchi *et al.*, 2016).

Which kinases phosphorylate such common sites? Candidates include CPKs which play critical roles during PTI and ETI (Boudsocq *et al.*, 2010; Gao *et al.*, 2013). Indeed, some of our identified common sites contain a CPK phosphorylation motif (S347 of RBOHD, S40 of PEN3 and S22 of ACA8, Tables S1–

S3). In particular, CPK10 was shown to phosphorylate synthetic peptides carrying S45 of PEN3 *in vitro* (Curran *et al.*, 2011), and CPK16 phosphorylates S22 of ACA8 *in vitro* (Giacometti *et al.*, 2012). However, the involvement of CPK10 and CPK16 in PTI and ETI is unknown. CPK4/5/6/11 have been shown to be required for the PAMP-inducible ROS burst (Boudsocq *et al.*, 2010; Dubiella *et al.*, 2013), and CPK1/2 have been shown to be required for full activation of the RPM1- and RPS2-mediated ROS burst (Gao *et al.*, 2013), suggesting the involvement of these CPKs in the phosphorylation of RBOHD during both PTI and ETI. CPK4/5/6/11 phosphorylate RBOHD at S163 and S347 *in vitro*, and these sites also encompass a CPK phosphorylation motif (Kadota *et al.*, 2014). CPK 2/4/11 also phosphorylate RBOHD at S148 *in vitro* (Gao *et al.*, 2013), but it is unknown whether CPK1/2 phosphorylate S163 and S347 *in vitro* or during ETI. The accumulating evidence suggests that multiple CPKs are involved in the phosphorylation of RBOHD and other defense components during PTI and ETI. However, as CPKs are unable to phosphorylate S343 (which does not possess a CPK phosphorylation motif) *in vitro* (Kadota *et al.*, 2014), it is likely that there are other kinase(s) that phosphorylate RBOHD during ETI (Fig. S6).

During PTI, the RLCK BIK1 phosphorylates RBOHD at residues S343 and S347 (Kadota *et al.*, 2014; Li *et al.*, 2014). This suggests that BIK1 or similar RLCKs might phosphorylate RBOHD during ETI. However, there is no current experimental evidence showing the involvement of BIK1 in ETI. Our data show that the *bik1pbl1* mutant does not affect RBOHD-mediated ROS production during ETI (Fig. 5). It is possible that other RLCKs act redundantly with BIK1 and PBL1 in the phosphorylation of RBOHD at S343 and S347 during ETI. Notably, RPS2 activation by AvrRpt2 induces the accumulation of many RLCKs, including BIK1, PBL2, PBL32 and RIPK, at 6 h after Dex treatment in *Dex:avrRpt2* plants (Elmore *et al.*, 2012). RPS2 activation by AvrRpt2 also induces the phosphorylation of RIPK at 3 h post-Dex treatment (Fig. 2), suggesting the possible involvement of RIPK in RPS2 signaling. It would be interesting to investigate the involvement of these RLCKs in RBOHD phosphorylation using multiple knockout mutants. Interestingly, the MAP4 kinase SIK1 has been found recently to be able to phosphorylate RBOHD during PTI (M. Zhang *et al.*, 2018). However, it remains to be elucidated whether SIK1 contributes to RBOHD phosphorylation during ETI.

MPK3 and MPK6 play critical roles in PTI and ETI signaling, and it is likely that these MPKs phosphorylate similar downstream proteins during PTI and ETI (Tsuda *et al.*, 2013; Su *et al.*, 2018). Examples of such proteins are WRKY transcription factors and 1-AMINO-CYCLOPROPANE-1-CARBOXYLIC ACID SYNTHASES (ACSs), which are the key enzymes of the ethylene biosynthesis pathway (Liu & Zhang, 2004; Adachi *et al.*, 2015; Sheikh *et al.*, 2016). In addition, in our dataset, for example, residues S63 of PEARLI4 and T336 of the CBS domain-containing protein contain an S/T-P MPK phosphorylation motif (Tables 1, S4). Hence, it is likely that MPKs, such as MPK3 and MPK6, phosphorylate these sites (Sorensson *et al.*, 2012).

MVQ1 is a negative regulator of WRKY-mediated defense gene expression during PTI and is phosphorylated on PAMP treatment (Pecher *et al.*, 2014). We found increased phosphorylation of S/T-P site S194 after activation of RPS2 (Table S1). Although direct evidence is not present, it is tempting to speculate that MVQ1 is phosphorylated during PTI and ETI by MPK3 and MPK6 to regulate WRKY-mediated gene expression.

The kinases phosphorylating common PTI and ETI phosphorylation sites *in vivo* are still largely unknown. The identification of these kinases is important in our understanding of how different receptors, localized to different cellular compartments, regulate the same defense components. Moreover, clarification of their activation mechanisms may further explain the commonalities and differences in PTI and ETI signaling. For example, differences in the dynamics and strength of kinase activation during PTI and ETI may cause differential phosphorylation dynamics of the defense components and subsequent immune signaling outputs (Tsuda *et al.*, 2013).

RPS2-regulated phosphorylation sites

In addition to common PTI and ETI phosphorylation sites, we identified undiscovered and novel phosphosites involved in RPS2 signaling. Some of these sites are located on important immune components, including PIP aquaporins. However, the kinases and phosphatases directly phosphorylating and dephosphorylating RPS2-regulated phosphosites remain largely unknown. CPKs and MPKs are strong candidate kinases for the phosphorylation of these sites because many RPS2-regulated phosphorylation sites contain CPK and/or MAPK phosphorylation motifs (Table S1). Some CPKs, including CPK1, phosphorylate synthetic peptides carrying S282 of PIP2D and T279 of PIP3 *in vitro*, both of which are RPS2-regulated phosphosites (Curran *et al.*, 2011). Further evidence comes from the RPS2-upregulated phosphosites, S11 of CALCIUM-BINDING EF-HAND FAMILY PROTEIN (AT2G41410) and S238 of ADAPTIN EAR-BINDING COAT-ASSOCIATED PROTEIN-1 (NECAP-1), which contain an S/T-P motif (Table S1). In addition, their phosphorylations were identified *in planta* after activation of MPK3/MPK6 by the expression of a constitutively active MEK^{DD} mutant protein (Hoehenwarter *et al.*, 2013). This suggests the possible involvement of MPK3/MPK6 in the phosphorylation of these residues. The identification and characterization of kinases and phosphatases regulating RPS2 signaling components, in addition to mutational analyses of the corresponding phosphorylation sites, would aid in the resolution of the RPS2 signaling network at the molecular level.

RBOHD-mediated ROS production is crucial for ETI

Our study revealed that RBOHD-mediated ROS production is required for resistance against avirulent bacteria, and thus for successful ETI. We also found that RBOHD-mediated ROS contributes to the resistance against a virulent fungus. A remaining question is how ROS contributes to the resistance against these pathogens. Although ROS are believed to be directly toxic to

pathogens (Lambeth, 2004), they are also likely to function as signaling molecules to change the redox status and affect the enzymatic activities and gene expression. In this context, it is interesting that PIPs, which transport H₂O₂ to the cytoplasm (Maurel *et al.*, 2015), are phosphorylated at activation sites during ETI (Figs 2, S3b; Table S4). This suggests that plants regulate the import of H₂O₂ produced via RBOHD, thereby actively altering the cellular redox status on ETI. In addition, the import of H₂O₂ through PIPs during ETI might, for example, induce stomatal closure, as these components play critical roles in stomatal closure (Kwak *et al.*, 2003; Mersmann *et al.*, 2010; Rodrigues *et al.*, 2017). Taken together, our data suggest that plants activate ROS production and ROS-mediated signaling occurs in large part by protein phosphorylation.

Final remarks

In summary, our study provides the first large-scale phosphoproteomic data of NLR-mediated ETI, adding important pieces to our understanding of the ETI signaling network. Among the identified differential phosphorylation sites, we found phosphorylation sites common to PTI and ETI signaling on a number of important defense-related proteins. Some of these phosphorylation sites play critical roles in the activation or inactivation of the corresponding proteins, and thereby mediate immune signaling. The observations made in this study enhance our understanding of immune signaling regulation during ETI and PTI. The future identification of proteins regulating the common phosphorylation sites, such as kinases, will further clarify the commonalities and differences of ETI and PTI at the molecular level.

Acknowledgements

We thank all the members of the Shirasu, Zipfel and Coaker laboratories for fruitful discussions, and the UC Davis proteomics core, Dr Mitch Elmore, Mrs Naomi Watanabe, Mrs Noriko Maki and Mrs Mamiko Kouzai for technical support. We also thank Dr Jian-Min Zhou for providing materials. This work was supported by the European Research Council (to CZ), The Gatsby Charitable Foundation (to CZ), MEXT/JSPS KAKENHI grant nos. JP16H06186 and JP16KT0037 (to YK), JP15H05959 and JP17H06172 (to KS), JP16J0071 (to YG), the National Institute of Health RO1GM092772 (to GC), the US Department of Agriculture USDA-NIFA 2015-67013-23082 (to GC) and the Ministerio de Economía y Competitividad of Spain (BIO2015-64077-R to AM and M-AT). TWHL was supported by a Rubicon grant of the Netherlands Organisation for Scientific Research (NWO).

Author contributions

GC, KS, CZ and AM supervised the research. TWHL performed the phosphoproteomic screen and experiments shown in Fig. S1. M-AT performed the fungus growth assay. YG performed the qRT-PCR analysis. JS, PD and FLHM performed the targeted phosphoproteomic analyses. YK performed the other

experiments. YK, TWHL, GC, CZ and KS wrote the manuscript. All the authors commented on the manuscript. YK and TWHL contributed equally to this work.

ORCID

Gitta Coaker  <http://orcid.org/0000-0003-0899-2449>
 Paul Derbyshire  <http://orcid.org/0000-0002-5095-9397>
 Yukihisa Goto  <http://orcid.org/0000-0003-3616-320X>
 Yasuhiro Kadota  <http://orcid.org/0000-0002-4782-1418>
 Thomas W. H. Liebrand  <http://orcid.org/0000-0003-1969-4148>
 Frank L. H. Menke  <http://orcid.org/0000-0003-2490-4824>
 Antonio Molina  <http://orcid.org/0000-0003-3137-7938>
 Ken Shirasu  <http://orcid.org/0000-0002-0349-3870>
 Jan Sklenar  <http://orcid.org/0000-0003-1858-2574>
 Miguel-Angel Torres  <http://orcid.org/0000-0002-0435-1786>
 Cyril Zipfel  <http://orcid.org/0000-0003-4935-8583>

References

- Adachi H, Nakano T, Miyagawa N, Ishihama N, Yoshioka M, Katou Y, Yaeno T, Shirasu K, Yoshioka H. 2015. WRKY transcription factors phosphorylated by MAPK regulate a plant immune NADPH oxidase in *Nicotiana benthamiana*. *Plant Cell* 27: 2645–2663.
- Benschop JJ, Mohammed S, O'Flaherty M, Heck AJ, Slijper M, Menke FL. 2007. Quantitative phosphoproteomics of early elicitor signaling in Arabidopsis. *Molecular & Cellular Proteomics: MCP* 6: 1198–1214.
- Boudsocq M, Willmann MR, McCormack M, Lee H, Shan L, He P, Bush J, Cheng SH, Sheen J. 2010. Differential innate immune signalling via Ca²⁺ sensor protein kinases. *Nature* 464: 418–422.
- Boutrot F, Zipfel C. 2017. Function, discovery, and exploitation of plant pattern recognition receptors for broad-spectrum disease resistance. *Annual Review of Phytopathology* 55: 257–286.
- Chakravorty D, Gookin TE, Milner MJ, Yu Y, Assmann SM. 2015. Extra-large G proteins expand the repertoire of subunits in Arabidopsis heterotrimeric G protein signaling. *Plant Physiology* 169: 512–529.
- Chaouch S, Queval G, Noctor G. 2012. AtRbohF is a crucial modulator of defence-associated metabolism and a key actor in the interplay between intracellular oxidative stress and pathogenesis responses in Arabidopsis. *Plant Journal* 69: 613–627.
- Chung EH, El-Kasbi F, He Y, Loehr A, Dangl JL. 2014. A plant phosphoswitch platform repeatedly targeted by type III effector proteins regulates the output of both tiers of plant immune receptors. *Cell Host & Microbe* 16: 484–494.
- Costa A, Luoni L, Marrano CA, Hashimoto K, Koster P, Giacometti S, De Michelis MI, Kudla J, Bonza MC. 2017. Ca²⁺-dependent phosphoregulation of the plasma membrane Ca²⁺-ATPase ACA8 modulates stimulus-induced calcium signatures. *Journal of Experimental Botany* 68: 3215–3230.
- Cui FH, Wu SJ, Sun WX, Coaker G, Kunkel B, He P, Shan LB. 2013. The *Pseudomonas syringae* Type III effector AvrRpt2 promotes pathogen virulence via stimulating Arabidopsis auxin/indole acetic acid protein turnover. *Plant Physiology* 162: 1018–1029.
- Curran A, Chang IF, Chang CL, Garg S, Miguel RM, Barron YD, Li Y, Romanowsky S, Cushman JC, Gribskov M *et al.* 2011. Calcium-dependent protein kinases from Arabidopsis show substrate specificity differences in an analysis of 103 substrates. *Frontiers in Plant Science* 2: 36.
- Dodds PN, Rathjen JP. 2010. Plant immunity: towards an integrated view of plant–pathogen interactions. *Nature Reviews Genetics* 11: 539–548.
- Dubiella U, Seybold H, Durian G, Komander E, Lässig R, Witte CP, Schulze WX, Romeis T. 2013. Calcium-dependent protein kinase/NADPH oxidase activation circuit is required for rapid defense signal propagation. *Proceedings of the National Academy of Sciences, USA* 110: 8744–8749.
- Elmore JM, Liu J, Smith B, Phinney B, Coaker G. 2012. Quantitative proteomics reveals dynamic changes in the plasma membrane during Arabidopsis immune signaling. *Molecular & Cellular Proteomics* 11: M111.014555.
- Frei dit Frey N, Mbengue M, Kwaaitaal M, Nitsch L, Altenbach D, Haweker H, Lozano-Duran R, Njo MF, Beekman T, Huettel B *et al.* 2012. Plasma membrane calcium ATPases are important components of receptor-mediated signaling in plant immune responses and development. *Plant Physiology* 159: 798–809.
- Gao X, Chen X, Lin W, Chen S, Lu D, Niu Y, Li L, Cheng C, McCormack M, Sheen J *et al.* 2013. Bifurcation of Arabidopsis NLR immune signaling via Ca²⁺-dependent protein kinases. *PLoS Pathogens* 9: e1003127.
- Giacometti S, Marrano CA, Bonza MC, Luoni L, Limonta M, De Michelis MI. 2012. Phosphorylation of serine residues in the N-terminus modulates the activity of ACA8, a plasma membrane Ca²⁺-ATPase of *Arabidopsis thaliana*. *Journal of Experimental Botany* 63: 1215–1224.
- He K, Gou X, Yuan T, Lin H, Asami T, Yoshida S, Russell SD, Li J. 2007. BAK1 and BKK1 regulate brassinosteroid-dependent growth and brassinosteroid-independent cell-death pathways. *Current Biology* 17: 1109–1115.
- Hernandez Sebastia C, Hardin SC, Clouse SD, Kieber JJ, Huber SC. 2004. Identification of a new motif for CDPK phosphorylation *in vitro* that suggests ACC synthase may be a CDPK substrate. *Archives of Biochemistry and Biophysics* 428: 81–91.
- Hoehenwarter W, Thomas M, Nukarinen E, Egelhofer V, Rohrig H, Weckwerth W, Conrath U, Beckers GJ. 2013. Identification of novel *in vivo* MAP kinase substrates in *Arabidopsis thaliana* through use of tandem metal oxide affinity chromatography. *Molecular & Cellular Proteomics: MCP* 12: 369–380.
- Huang JZ, Hardin SC, Huber SC. 2001. Identification of a novel phosphorylation motif for CDPKs: phosphorylation of synthetic peptides lacking basic residues at P-3/P-4. *Archives of Biochemistry and Biophysics* 393: 61–66.
- Huang JZ, Huber SC. 2001. Phosphorylation of synthetic peptides by a CDPK and plant SNF1-related protein kinase. Influence of proline and basic amino acid residues at selected positions. *Plant and Cell Physiology* 42: 1079–1087.
- Johansson ON, Fantozzi E, Fahlberg P, Nilsson AK, Buhot N, Tor M, Andersson MX. 2014. Role of the penetration-resistance genes *PEN1*, *PEN2* and *PEN3* in the hypersensitive response and race-specific resistance in *Arabidopsis thaliana*. *Plant Journal* 79: 466–476.
- Jones AM, Bennett MH, Mansfield JW, Grant M. 2006. Analysis of the defence phosphoproteome of *Arabidopsis thaliana* using differential mass tagging. *Proteomics* 6: 4155–4165.
- Jones JD, Dangl JL. 2006. The plant immune system. *Nature* 444: 323–329.
- Kadota Y, Shirasu K, Zipfel C. 2015. Regulation of the NADPH oxidase RBOHD during plant immunity. *Plant and Cell Physiology* 56: 1472–1480.
- Kadota Y, Sklenar J, Derbyshire P, Stransfeld L, Asai S, Ntoukakis V, Jones JD, Shirasu K, Menke F, Jones A *et al.* 2014. Direct regulation of the NADPH oxidase RBOHD by the PRR-associated kinase BIK1 during plant immunity. *Molecular Cell* 54: 43–55.
- Kemmerling B, Schwedt A, Rodriguez P, Mazzotta S, Frank M, Qamar SA, Mengiste T, Betsuyaku S, Parker JE, Mussig C *et al.* 2007. The BRI1-associated kinase 1, BAK1, has a brassinolide-independent role in plant cell-death control. *Current Biology* 17: 1116–1122.
- Khan M, Subramaniam R, Desveaux D. 2016. Of guards, decoys, baits and traps: pathogen perception in plants by type III effector sensors. *Current Opinion in Microbiology* 29: 49–55.
- Kim MG, da Cunha L, McFall AJ, Belkadir Y, DebRoy S, Dangl JL, Mackey D. 2005. Two *Pseudomonas syringae* type III effectors inhibit RIN4-regulated basal defense in Arabidopsis. *Cell* 121: 749–759.
- Kim MG, Geng X, Lee SY, Mackey D. 2009. The *Pseudomonas syringae* type III effector AvrRpm1 induces significant defenses by activating the Arabidopsis nucleotide-binding leucine-rich repeat protein RPS2. *Plant Journal* 57: 645–653.

- Kwak JM, Mori IC, Pei ZM, Leonhardt N, Torres MA, Dangl JL, Bloom RE, Bodde S, Jones JD, Schroeder JI. 2003. NADPH oxidase *AtrbohD* and *AtrbohF* genes function in ROS-dependent ABA signaling in Arabidopsis. *EMBO Journal* 22: 2623–2633.
- Kwon C, Bednarek P, Schulze-Lefert P. 2008. Secretory pathways in plant immune responses. *Plant Physiology* 147: 1575–1583.
- Lambeth JD. 2004. NOX enzymes and the biology of reactive oxygen. *Nature Reviews Immunology* 4: 181–189.
- Lee D, Bourdais G, Yu G, Robatzek S, Coaker G. 2015. Phosphorylation of the plant immune regulator RPM1-INTERACTING PROTEIN4 enhances plant plasma membrane H⁺-ATPase activity and inhibits flagellin-triggered immune responses in Arabidopsis. *Plant Cell* 27: 2042–2056.
- Li L, Li M, Yu L, Zhou Z, Liang X, Liu Z, Cai G, Gao L, Zhang X, Wang Y *et al.* 2014. The FLS2-associated kinase BIK1 directly phosphorylates the NADPH oxidase RbohD to control plant immunity. *Cell Host & Microbe* 15: 329–338.
- Liang X, Ding P, Lian K, Wang J, Ma M, Li L, Li L, Li M, Zhang X, Chen S *et al.* 2016. Arabidopsis heterotrimeric G proteins regulate immunity by directly coupling to the FLS2 receptor. *eLife* 5: e13568.
- Liu J, Elmore JM, Lin ZJ, Coaker G. 2011. A receptor-like cytoplasmic kinase phosphorylates the host target RIN4, leading to the activation of a plant innate immune receptor. *Cell Host & Microbe* 9: 137–146.
- Liu Y, Zhang S. 2004. Phosphorylation of 1-aminocyclopropane-1-carboxylic acid synthase by MPK6, a stress-responsive mitogen-activated protein kinase, induces ethylene biosynthesis in Arabidopsis. *Plant Cell* 16: 3386–3399.
- Lofke C, Luschig C, Kleine-Vehn J. 2013. Posttranslational modification and trafficking of PIN auxin efflux carriers. *Mechanisms of Development* 130: 82–94.
- Lolle S, Greff C, Petersen K, Roux M, Jensen MK, Bressendorff S, Rodriguez E, Somark K, Mundy J, Petersen M. 2017. Matching NLR immune receptors to autoimmunity in *camta3* mutants using antimorphic NLR alleles. *Cell Host & Microbe* 21: 518–529.
- Marino D, Dunand C, Puppo A, Pauly N. 2012. A burst of plant NADPH oxidases. *Trends in Plant Science* 17: 9–15.
- Mattei B, Spinelli F, Pontiggia D, De Lorenzo G. 2016. Comprehensive analysis of the membrane phosphoproteome regulated by oligogalacturonides in *Arabidopsis thaliana*. *Frontiers in Plant Science* 7: 1107.
- Maurel C, Boursiac Y, Luu DT, Santoni V, Shahzad Z, Verdoucq L. 2015. Aquaporins in plants. *Physiological Reviews* 95: 1321–1358.
- McNellis TW, Mudgett MB, Li K, Aoyama T, Horvath D, Chua NH, Staskawicz BJ. 1998. Glucocorticoid-inducible expression of a bacterial avirulence gene in transgenic Arabidopsis induces hypersensitive cell death. *Plant Journal* 14: 247–257.
- Mersmann S, Bourdais G, Rietz S, Robatzek S. 2010. Ethylene signaling regulates accumulation of the FLS2 receptor and is required for the oxidative burst contributing to plant immunity. *Plant Physiology* 154: 391–400.
- Mine A, Seyfferth C, Kracher B, Berens ML, Becker D, Tsuda K. 2018. The defense phytohormone signaling network enables rapid, high-amplitude transcriptional reprogramming during effector-triggered immunity. *Plant Cell* 30: 1199–1219.
- Morales J, Kadota Y, Zipfel C, Molina A, Torres MA. 2016. The Arabidopsis NADPH oxidases RbohD and RbohF display differential expression patterns and contributions during plant immunity. *Journal of Experimental Botany* 67: 1663–1676.
- Morsomme P, Boutry M. 2000. The plant plasma membrane H⁺-ATPase: structure, function and regulation. *Biochimica et Biophysica Acta* 1465: 1–16.
- Nishimura MT, Stein M, Hou BH, Vogel JP, Edwards H, Somerville SC. 2003. Loss of a callose synthase results in salicylic acid-dependent disease resistance. *Science* 301: 969–972.
- Nühse TS, Bottrill AR, Jones AME, Peck SC. 2007. Quantitative phosphoproteomic analysis of plasma membrane proteins reveals regulatory mechanisms of plant innate immune responses. *Plant Journal* 51: 931–940.
- Pecher P, Eschen-Lippold L, Herklotz S, Kuhle K, Naumann K, Bethke G, Uhrig J, Weyhe M, Scheel D, Lee J. 2014. The Arabidopsis thaliana mitogen-activated protein kinases MPK3 and MPK6 target a subclass of 'VQ'-motif-containing proteins to regulate immune responses. *New Phytologist* 203: 592–606.
- Petersen M, Brodersen P, Naested H, Andreasson E, Lindhart U, Johansen B, Nielsen HB, Lacy M, Austin MJ, Parker JE *et al.* 2000. Arabidopsis map kinase 4 negatively regulates systemic acquired resistance. *Cell* 103: 1111–1120.
- Piasecka A, Jedrzejczak-Rey N, Bednarek P. 2015. Secondary metabolites in plant innate immunity: conserved function of divergent chemicals. *New Phytologist* 206: 948–964.
- Pogany M, von Rad U, Grun S, Dongo A, Pintye A, Simoneau P, Bahnweg G, Kiss L, Barna B, Durner J. 2009. Dual roles of reactive oxygen species and NADPH oxidase RBOHD in an Arabidopsis–*Alternaria* pathosystem. *Plant Physiology* 151: 1459–1475.
- Qi Y, Katagiri F. 2009. Purification of low-abundance Arabidopsis plasma-membrane protein complexes and identification of candidate components. *Plant Journal* 57: 932–944.
- Rayapuram N, Bonhomme L, Bigeard J, Haddadou K, Przybylski C, Hirt H, Pflieger D. 2014. Identification of novel PAMP-triggered phosphorylation and dephosphorylation events in *Arabidopsis thaliana* by quantitative phosphoproteomic analysis. *Journal of Proteome Research* 13: 2137–2151.
- Rodrigues O, Reshetnyak G, Grondin A, Saijo Y, Leonhardt N, Maurel C, Verdoucq L. 2017. Aquaporins facilitate hydrogen peroxide entry into guard cells to mediate ABA- and pathogen-triggered stomatal closure. *Proceedings of the National Academy of Sciences, USA* 114: 9200–9205.
- Sheikh AH, Eschen-Lippold L, Pecher P, Hoehenwarter W, Sinha AK, Scheel D, Lee J. 2016. Regulation of WRKY46 transcription factor function by mitogen-activated protein kinases in *Arabidopsis thaliana*. *Frontiers in Plant Science* 7: 61.
- Sorensson C, Lenman M, Veide-Vilg J, Schopper S, Ljungdahl T, Groth M, Tamas MJ, Peck SC, Andreasson E. 2012. Determination of primary sequence specificity of Arabidopsis MAPKs MPK3 and MPK6 leads to identification of new substrates. *Biochemical Journal* 446: 271–278.
- Spoel SH, Dong X. 2012. How do plants achieve immunity? Defence without specialized immune cells. *Nature Reviews Immunology* 12: 89–100.
- Su J, Yang L, Zhu Q, Wu H, He Y, Liu Y, Xu J, Jiang D, Zhang S. 2018. Active photosynthetic inhibition mediated by MPK3/MPK6 is critical to effector-triggered immunity. *PLoS Biology* 16: e2004122.
- Suzuki N, Miller G, Morales J, Shulaev V, Torres MA, Mittler R. 2011. Respiratory burst oxidases: the engines of ROS signaling. *Current Opinion in Plant Biology* 14: 691–699.
- Svnenelid F, Olsson A, Piotrowski M, Rosenquist M, Ottman C, Larsson C, Oecking C, Sommarin M. 1999. Phosphorylation of Thr-948 at the C terminus of the plasma membrane H⁺-ATPase creates a binding site for the regulatory 14-3-3 protein. *Plant Cell* 11: 2379–2391.
- Takeda S, Gapper C, Kaya H, Bell E, Kuchitsu K, Dolan L. 2008. Local positive feedback regulation determines cell shape in root hair cells. *Science* 319: 1241–1244.
- Thaler JS, Humphrey PT, Whiteman NK. 2012. Evolution of jasmonate and salicylate signal crosstalk. *Trends in Plant Science* 17: 260–270.
- Thomma BP, Nurnberger T, Joosten MH. 2011. Of PAMPs and effectors: the blurred PTI–ETI dichotomy. *Plant Cell* 23: 4–15.
- Thordal-Christensen H, Zhang Z, Wei Y, Collinge DB. 1997. Subcellular localization of H₂O₂ in plants. H₂O₂ accumulation in papillae and hypersensitive response during the barley–powdery mildew interaction. *Plant Journal* 11: 1187–1194.
- Tian S, Wang X, Li P, Wang H, Ji H, Xie J, Qiu Q, Shen D, Dong H. 2016. Plant aquaporin AtPIP1;4 links apoplastic H₂O₂ induction to disease immunity pathways. *Plant Physiology* 171: 1635–1650.
- Torres MA, Dangl JL, Jones JD. 2002. Arabidopsis gp91phox homologues AtrbohD and AtrbohF are required for accumulation of reactive oxygen intermediates in the plant defense response. *Proceedings of the National Academy of Sciences, USA* 99: 517–522.
- Torres MA, Morales J, Sanchez-Rodriguez C, Molina A, Dangl JL. 2013. Functional interplay between Arabidopsis NADPH oxidases and heterotrimeric G protein. *Molecular Plant–Microbe Interactions* 26: 686–694.
- Tsuda K, Katagiri F. 2010. Comparing signaling mechanisms engaged in pattern-triggered and effector-triggered immunity. *Current Opinion in Plant Biology* 13: 459–465.
- Tsuda K, Mine A, Bethke G, Igarashi D, Botanga CJ, Tsuda Y, Glazebrook J, Sato M, Katagiri F. 2013. Dual regulation of gene expression mediated by extended MAPK activation and salicylic acid contributes to robust innate immunity in *Arabidopsis thaliana*. *PLoS Genetics* 9: e1004015.

- Tyanova S, Temu T, Cox J. 2016a. The MaxQuant computational platform for mass spectrometry-based shotgun proteomics. *Nature Protocols* 11: 2301–2319.
- Tyanova S, Temu T, Sinitcyn P, Carlson A, Hein MY, Geiger T, Mann M, Cox J. 2016b. The Perseus computational platform for comprehensive analysis of (prote)omics data. *Nature Methods* 13: 731–740.
- Underwood W, Somerville SC. 2017. Phosphorylation is required for the pathogen defense function of the Arabidopsis PEN3 ABC transporter. *Plant Signal Behav* 12: e1379644.
- Vizcaino JA, Cote RG, Csordas A, Dienes JA, Fabregat A, Foster JM, Griss J, Alpi E, Birim M, Contell J *et al.* 2013. The PRoteomics IDentifications (PRIDE) database and associated tools: status in 2013. *Nucleic Acids Research* 41: D1063–D1069.
- Wang J, Grubb LE, Wang J, Liang X, Li L, Gao C, Ma M, Feng F, Li M, Li L *et al.* 2018. A regulatory module controlling homeostasis of a plant immune kinase. *Molecular Cell* 69: 493–504.
- Xin XF, Nomura K, Aung K, Velasquez AC, Yao J, Boutrot F, Chang JH, Zipfel C, He SY. 2016. Bacteria establish an aqueous living space in plants crucial for virulence. *Nature* 539: 524–529.
- Yamauchi S, Takemiya A, Sakamoto T, Kurata T, Tsutsumi T, Kinoshita T, Shimazaki K. 2016. The plasma membrane H⁺-ATPase AHA1 plays a major role in stomatal opening in response to blue light. *Plant Physiology* 171: 2731–2743.
- Yu X, Feng B, He P, Shan L. 2017. From chaos to harmony: responses and signaling upon microbial pattern recognition. *Annual Review of Phytopathology* 55: 109–137.
- Zhang J, Li W, Xiang T, Liu Z, Laluk K, Ding X, Zou Y, Gao M, Zhang X, Chen S *et al.* 2010. Receptor-like cytoplasmic kinases integrate signaling from multiple plant immune receptors and are targeted by a *Pseudomonas syringae* effector. *Cell Host & Microbe* 7: 290–301.
- Zhang M, Chiang Y-H, Toruño TY, Lee D, Ma M, Liang X, Lal NK, Lemos M, Lu Y-J, Ma S *et al.* 2018. The MAP4 kinase SIK1 ensures robust extracellular ROS burst and antibacterial immunity in plants. *Cell Host & Microbe* 24: 379–391.
- Zhang Z, Liu Y, Huang H, Gao M, Wu D, Kong Q, Zhang Y. 2017. The NLR protein SUMM2 senses the disruption of an immune signaling MAP kinase cascade via CRCK3. *EMBO Reports* 18: 292–302.
- Zhang Z, Wu Y, Gao M, Zhang J, Kong Q, Liu Y, Ba H, Zhou J, Zhang Y. 2012. Disruption of PAMP-induced MAP kinase cascade by a *Pseudomonas syringae* effector activates plant immunity mediated by the NB-LRR protein SUMM2. *Cell Host & Microbe* 11: 253–263.
- Zhu H, Li GJ, Ding L, Cui X, Berg H, Assmann SM, Xia Y. 2009. Arabidopsis extra large G-protein 2 (XLG2) interacts with the Gbeta subunit of heterotrimeric G protein and functions in disease resistance. *Molecular Plant* 2: 513–525.

Supporting Information

Additional Supporting Information may be found online in the Supporting Information section at the end of the article.

Fig. S1 Dexamethasone (Dex)-inducible *avrRpt2* expression in *Arabidopsis*.

Fig. S2 Alignments of differentially phosphorylated sites in PLASMA MEMBRANE INTRINSIC PROTEIN (PIP), H⁺-ATPase (AHA) and PIN-FORMED (PIN) proteins.

Fig. S3 RESPIRATORY BURST OXIDASE HOMOLOG D (RBOHD) phosphorylation sites S343 and S347 are required for

flagellin 22 (*flg22*)-inducible reactive oxygen species (ROS) burst.

Fig. S4 Conservation of identified RESPIRATORY BURST OXIDASE HOMOLOG D (RBOHD) phosphorylation sites in the phosphoproteomic screen.

Fig. S5 The *rbohD/pRBOHD:3xFLAG-RBOHD* (*S343A/S347A*) complementation line is resistant to *Plectosphaerella cucumerina* (*PcBMM* isolate).

Fig. S6 Schematic representation of RESISTANT TO *P. SYRINGAE*-2 (RPS2) domains and the phosphorylation sites during pathogen-associated molecular pattern (PAMP)-triggered immunity (PTI) and effector-triggered immunity (ETI).

Methods S1 Supplementary methods describing materials, phosphoproteomic analysis, reactive oxygen species (ROS) assay, quantitative reverse transcription-polymerase chain reaction (qRT-PCR), western blotting and disease assays.

Table S1 Summary of significantly differentially phosphorylated sites and corresponding protein levels.

Table S2 Summary of RESISTANT TO *P. SYRINGAE*-2 (RPS2)-upregulated phosphorylation sites.

Table S3 Summary of RESISTANT TO *P. SYRINGAE*-2 (RPS2)-downregulated phosphorylation sites.

Table S4 Summary of the phosphorylation sites discussed in this article.

Table S5 Maxquant search parameters for LC-MS/MS data analysis.

Table S6 MS1 intensities and MS/MS counts for selected phosphorylation sites.

Table S7 Specific transitions used for selected reaction monitoring (SRM) on RESPIRATORY BURST OXIDASE HOMOLOG D (RBOHD).

Table S8 Primers used in this study.

Please note: Wiley Blackwell are not responsible for the content or functionality of any Supporting Information supplied by the authors. Any queries (other than missing material) should be directed to the *New Phytologist* Central Office.